


TU Wien - UPC

Master Thesis

Experimental investigation on carbon dioxide dissolution in saline aquifers

Author:
Carlos Salinas

Supervisor:
Marco De Paoli

A thesis submitted in fulfillment of the requirements for the Master Thesis

in the

Institute of Fluid Mechanics and Heat Transfer

July 10, 2018

TU WIEN - UPC

Abstract

ETSEIB
Institute of Fluid Mechanics and Heat Transfer

Master Thesis

Experimental investigation on carbon dioxide dissolution in saline aquifers

by Carlos SALINAS

Since the industrial development has become one of the main factors in human's life, carbon dioxide (CO_2) emissions to the atmosphere has increased considerably over the last 40 years. This enhancement represents one of the main issues that governments are concerned about because of its effects and consequences, known as greenhouse effect. In order to reduce the quantity of CO_2 in the atmosphere, different strategies are proposed, studied and applied. One of them consists in injecting the gas in underground geological formations, with the aim of keeping it there safely and as long as possible. One of the trapping mechanisms that play a key role in this storage process is the solubility trapping.

In this thesis, related to the experimental investigation on this mechanism, potassium permanganate ($KMnO_4$) is used to investigate the dissolution dynamics of CO_2 in water. This chemical component has been chosen instead of CO_2 due to its benefits: similar properties in less severe environmental conditions (pressure and temperature) in the laboratory, no need to use a porous media (this is the media underground) to get a better analysis of the experiments and the time required to run the experiments (hours in $KMnO_4$ case whereas hundreds of years in CO_2).

In this thesis the procedure followed to simulate the real process of mixture between both substances, accomplished in a Hele Shaw cell is explained. It has been derived a relationship between the mass fraction of the solution and the light intensity of the pictures taken, an essential step in order to analyse the images. This process is totally experimental. We identified the best configuration to initiate the mixture without disturbances and be as more representative as possible of the real process. And finally, we have also compared the results obtained, distinguishing 3 regimes (diffusive, constant and shutdown) with the results got, numerically, by De Paoli *et al.* (2017). The influence of the Rayleigh number on the regimes, in particular on their onset, requires further investigations and is left for future work.

Acknowledgements

I wish to thank, first of all, the person that has guided all my project and has been my supervisor during all the thesis: Marco De Paoli. Many thanks for allowing me to participate in his investigation group, for permitting me get into the Institute of Fluid Mechanics and Heat Transfer of the Technische Universität of Wien, for trusting on me at from the beginning, before arriving Wien and to accept my proposal and for his selfless help about all the topics that I have could have doubts.

I would like to express my true gratitude to Mobin Alipour, member of the same department and student of PhD, for his helping during all the project, being always available to resolve my doubts and collaborating during the experiments. A special mention to Atahan Kap and Kaan Kurt, bachelor students of TU Wien, due to their collaboration during all the experiments in the laboratory.

I would also like to express my heartfelt gratitude to Jordi Biosca, because he has always offered to me his help and knowledge about software *Matlab* when I required its assistance.

And finally, but by no means least, my gratitude goes out to my family and my girlfriend, for their support, not only right now, but during all the bachelor and the master, allowing to me to grow as a person and trusting all time on me. Thank you.

Contents

List of Figures

List of Tables

Chapter 1

Introduction

In order to understand the motivation of this work, it is essential to talk about carbon dioxide (CO_2) effect into atmosphere, which are its consequences and how this big and alarming trouble could be fixed.

1.1 Greenhouse effect and climate change

The world changed after industrial revolution in 18^{th} century, and specially the industrial progress increased the number of machines, facilitating people's life. However, this development is associated to side effects like contamination, and mainly CO_2 emissions and consequently, greenhouse effect. The technology that has been developing has become more and more dependent on fossil fuels such as coal, petroleum oil and natural gas, until the point that approximately 85% of the world's energy demand is supplied by fossil fuel combustion.

The problem that CO_2 produces is it absorbs infrared radiation, avoiding that it could be release to the space and retaining it within the Earth's atmosphere. And this radiation stack warms the Earth, rising up its temperature. This effect is named "greenhouse effect". The consequences are terrible: global temperature increases, polar ice caps melt, climatic instability, health public problems and food degradation risk, according to OMS reports (Sucasas, 2018). These are just a few examples of the problems that it causes. Figure 1.1 shows the relationship between CO_2 and temperature and how both have been increasing since 18^{th} century.

Therefore, it is understood that nowadays, CO_2 emissions poured into the atmosphere is one of the main issues different global governments are worried about, in

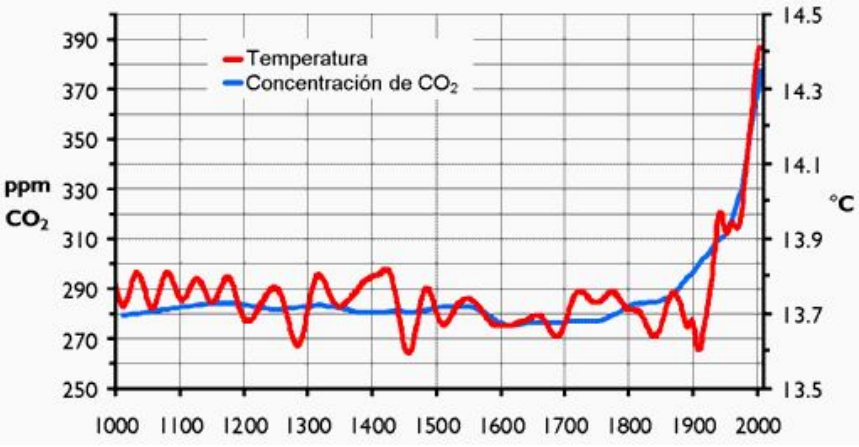

FIGURE 1.1: Progress of averaged air temperature and CO_2 concentration into the atmosphere since 1000 until nowadays (Gorrini, 2007).

order to stop greenhouse effect, caused by this gas. However, instead of the measurements taken and different meetings with political representatives from the most important countries in the world (one of the last meetings was in Bonn in November 2017) in order to fix this problem, the current fact says that last year, CO_2 emissions spilled into the atmosphere rose 2% (Sucasas, 2018), being this values catastrophic.

China, United States of America, India, Russia and Germany, respectively, are the main carbon dioxide emitting countries, with almost $20.000 \cdot 10^9$ Mt annually, which represents almost 59% of the global amount (CIA, 2015). Although countries as Germany, for example, are dropping its amount each year (Gapminder, 2018), the politics develop by countries as China or USA trusting in fossil fuel as the main energy resource instead of renewable energies or nuclear power plants (remind that nuclear power plants do not produce CO_2) warm this values could even be double in little more than 20 years.

Increasing even more CO_2 level in atmosphere, climate change (or Earth's temperature) will increment, and it is expected that it affects the well-being of millions of people through increased malnutrition and spread of infectious diseases, and rise mortality up due to hate waves, wildfires, storms floods and droughts. But even CO_2 are stabilized and kept constant, average global surface temperature is expected a further warming of $0,1$ °C per decade (Cherezov, 2017). So the priority is not just reducing the emissions, but to reduce the accumulation that is now in the atmosphere.

Therefore, to fix greenhouse effect issue, there are 3 different alternatives: emit less quantity, but this fact is unlikely nowadays in spite of some government efforts and renewable energies growth; sequestrate it in order to be treated afterwards and reuse it to create new products (Repsol company has got a plastic made of CO_2); sequestrate and store it underground. Of this chances, the work will be focus on the third one, and concretely, the storage.

1.2 Carbon dioxide capture and storage

In order to facilitate the gas capture, CO_2 has to be produced by large point sources such as fossil power plants (instead of, e.g. cars oil combustion), where coal, oil or natural gas is burnt, and other large-scale industrial processes such as iron, steel and ammonia manufacturing. In order to transport carbon dioxide, it has to be produced at high pressure. Carbon capture sequestration (CSS) option enables keep using fossil fuels to produce energy until renewable and nuclear sources could supply completely energy world demand.

Nowadays, three technologies enables CO_2 capture: post-combustion capture, pre-combustion capture and oxyfuel combustion. Depending on the type of plant, it is chosen a method. Post-combustion capture consists on separating different combustion gases contained in the flue using physical or chemical solvents and membranes. Pre-combustion capture is applicable to integrated gasification combined cycle power plants (IGCC), where carbon is captured from syngas, which it is a gas obtained of substances with high content in carbon subject to a high temperature chemical process, before its combustion (DOE, 2018). Finally, oxyfuel combustion uses pure oxygen during combustion, what let that gases contain in chimney are mostly water and CO_2. The first process is the best understood method and it has the advantage that it is possible to be adjusted to existing plants since this method does not modify the combustion process. Subsequently CO_2 is injected beneath the surface of the Earth.

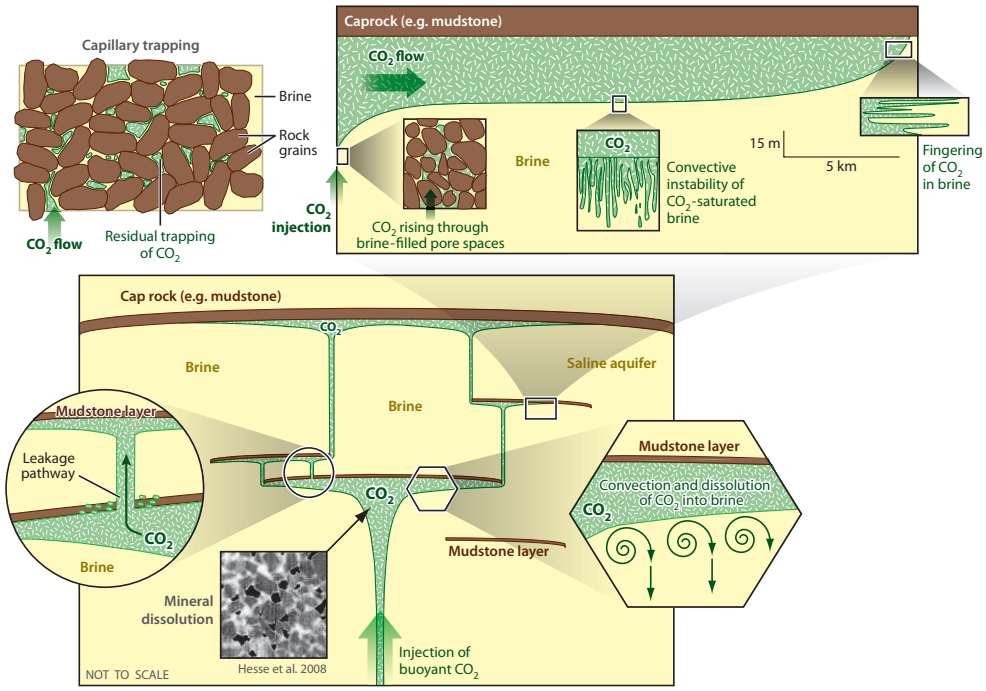

FIGURE 1.2: Overview of the fluid dynamics associated with the geological storage of CO_2, including buoyancy-driven spreading, leakage, and residual trapping due to dissolution and capillary trapping. Courtesy of Huppert & Neufeld (2014).

If we talk about storage, CO_2 could be reserved in deep oceans or mineral carbonation. But this option is still in development, besides the risks on marine ecosystems are big and carbon dioxide conversion in inorganic matter would cause an important impact on environment due to the substances required. High cost is also a issue. However, geological sequestration is a viable option. Actually, there are different projects running this procedure, but they will be explained later in subsection 1.3. Possible available reservoirs for CO_2 include old oil reservoirs and saline aquifers, in which the largest storage potential is thought to exist. Especially for the second ones, it is estimated that their capacity is between 1.000 and 10.000 billion tonnes of liquefied carbon dioxide. Moreover, technology needs to inject CO_2 is already in use in oil and gas industries. And in addition, how the liquid inside saline aquifers is brine (no potable water), it can not be used for daily applications (at least without a treatment) so it does not suppose an issue related to "contaminated" it. The main risk are leakages that emit back CO_2 into the atmosphere, which means that really big efforts and money would be wasted.

The injection of CO_2 into saline aquifers is typically envisaged at depths between 800 and 3.000 m. At this depths, CO_2 exists in a supercritical state, and its density could vary between 600 and 800 kg/m^3, in comparison with 2 kg/m^3 of the same gas at atmospheric conditions. On the other hand, at these depths beneath the surface of the Earth, the predominant substance is brine, whose density is approximately 1000 km/m^3. Thus, if carbon dioxide is injected, density difference between both fluids would make the less dense element (CO_2 in our case) flows to the top, being storage just under the rock layer. This situation is undesirable because if the layer was broken due to an unpredictable fact, the gas would be released back into the atmosphere, and all energy, time and money inverted would be useless. That is the main reason why

CO_2 treatment will be found. It is important to remind that the aim is to sequestrate CO_2 for as much time as possible. A second choice consist in introducing the gas in a rock ground and trap carbon dioxide between the gap stones. However, if some ground movements where produced, the gas would rise again to the upper crust part and we would have the same issue before mentioned. So, it is necessary to find a way to store safely and for long time the gas (hundreds of years), without any option of leakages to the atmosphere, and it consists in getting a brine-CO_2 mixture. As mentioned before, brine's density is approximately 1000 kg/m^3, whereas mixture density would be a bit higher, around 1050 kg/m^3. In this way, the mixture flows to the bottom, due to its heavier density, and CO_2 won't remain close to the layer, and all the zone will be covered by the dissolution, because density difference is not big enough to keep brine at the upper and mixture at the bottom.

This last configuration will be the object of the present study. In order to investigate these dissolution dynamics, a Hele-Shaw cell will be used. Experimentally, the aim is to observe the behaviour of the mixture, and how the dissolution fingers develop, to use afterwards a software and study the results got, to ensure later safe, long term storage. Figure 1.2 shows the 3 different trapping mechanisms. The circle image illustrates how CO_2 rises up when dissolution does not occur, until making a layer behind the caprock. Left upper part displays how CO_2 is trapped in the rocks (capillary trapping). Finally, the hexagonal window shows that brine-CO_2 mixture flows down, insuring carbon dioxide will not be released. It is important emphasize that in each situation, fluid dynamics runs elements behaviours.

1.3 Current state and future developments of CCS plants and projects

Different projects and plants are Currently involved in CO_2 capture and sequestration. There are 17 large scale facilities operating in the world that save 37 million of tonnes each year of being spilled to the atmosphere (Otiniando Pulido, 2018). The majority of this plants are in the United States. And it is because American oil companies use CO_2 in order to extract the whole amount of oil that there is inside reservoirs. Without injecting this gas, only about 50% of oil can be extract. Then, this procedure has two benefits: extract oil and storage CO_2, since it is sequestrated inside reservoir. This process is also called Enhanced Oil Recovery. This explains why some companies works with CCS since 1972 (Table 1.1). However, the process of capture, inject and store CO_2 is not cheap, and some industries reject them because of money, since if there is not a direct advantage (extract oil), they prefer pay for emission trading. But in last years, since the importance of sequestrating this gas has increased, so many companies try to do it and technologies and facilities are growing up, just like investigations about them. Now we sum up all large scale CCS facilities that are working nowadays (Table 1.1), which are in construction (Table 1.2), in advanced development (Table 1.3) and in early development (Table 1.4), indicating where they are built or supposed to, its capacity and year since they are operating or they expect start operating. All this data has been extract of Institute (n.d.).

TABLE 1.1: Current large scale CCS facilities around the world.

Country	**District**	**CO_2 capture capacity [Mtpa]**	**Operation date**
United States	Texas	0,4-0,5	1972
United States	Oklahoma	0,7	1982
United States	Wyoming	7	1986
Norway	North sea	1	1996
Canada	Saskatchewan	3	2000
Norway	Barents Sea	0,7	2008
United States	Texas	8,4	2010
United States	Texas	1	2013
United States	Kansas	1	2013
United States	Wyoming	0,9	2013
Brazil	Santos Basin	~ 1	2013
Canada	Saskatchewan	1	2014
Saudi Arabia	Eastern Province	0,8	2015
Canada	Alberta	~ 1	2015
United Arab Emirates	Abu Dhabi	0,8	2016
United States	Texas	1,4	2017
United States	Illinois	1	2017

TABLE 1.2: Large scale CCS facilities in construction around the world.

Country	**District**	**CO_2 capture capacity [Mtpa]**	**Operation date**
Australia	Western Australia	3,4 - 4	2018
Canada	Alberta	0,3 - 0,6	2018
Canada	Alberta	1,2 - 1,4	2018
China	Shandong Province	0,4	2019
China	Shaanxi Province	0,41	2020

TABLE 1.3: Large scale CCS facilities in advanced development around the world.

Country	**District**	**CO_2 capture capacity [Mtpa]**	**Operation date**
United States	Louisiana	4,2	2022
United States	Texas	1,5 - 2	2022
Norway	Southern Norway	1,2	2022
Australia	Victoria	0,5 - 1	2020's

It is interesting see although USA is the country with more facilities operating (9 out of 17), only 2 out of 20 projects in construction or development belong to them, and the explanation is that their aim is extract fossil fuels. It is also interesting how Australia and Eastern Asia do not have any project working at the present state, but 13 out of 20 future plants will be located there. Finally, in Europe, only Norway has this kind of plants, taking advantage of his proximity to the sea, although United Kingdom has started to interest in this projects, being still soon until they start operating.

TABLE 1.4: Current large scale CCS facilities in early development around the world.

Country	**District**	**CO_2 capture capacity [Mtpa]**	**Operation date**
China	Jiiangsu Province	0,5	2020-2021
China	Shandong Province	1	2020's
China	Guangdong Province	1	2020's
China	Tanjin	2	2020's
China	Shanxi Province	2	2020's
China	Ningxia Hui Region	2	2020's
South Korea	Chungnam Province	1	2020's
South Korea	Not decided	1	2020's
United Kingdom	Tees Valley	0,8	2020's
United Kingdom	Scotland	3	2024
Australia	Western Australia	2,5	2025

1.4 Trapping mechanisms

We know trapping mechanisms as the process by means of natural oil or gases are immobilized beneath the Earth surface, so many times as a natural process. They involve physical, chemical and mechanical reactions. We talk about CO_2, so in the following subsections these mechanisms, applied to carbon dioxide, are explained.

1.4.1 Capillary trapping

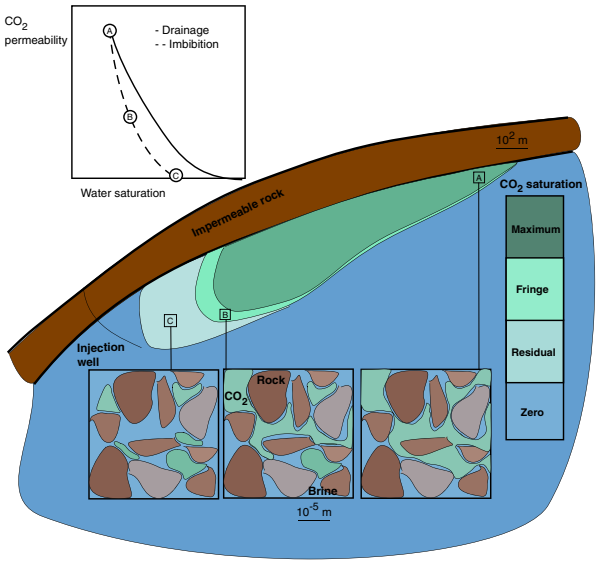

FIGURE 1.3: A sketch of key processes governed by capillary trapping after CO_2 injection has ceased at a storage site (Krevor *et al.*, 2015).

Carbon dioxide trapping by capillary forces in the pore space of rocks is a key method to maximize storage capacity. When the gas is injected into a deep surface geologic formation, it will displace the fluid contained inside, generally brine, and migrate in response to buoyancy and pressure gradients. As the reservoir brine imbibes back into the pore space pursuant to migrating CO_2 plume, small isolated blobs of CO_2 will be trapped. It is known as capillary or residual trapping. In Figure 1.3 is illustrated the configuration. The isolated blobs size is similar to rocks pores, and fluid physics and interfacial forces govern the process (Krevor *et al.*, 2015).

1.4.2 Solubility trapping

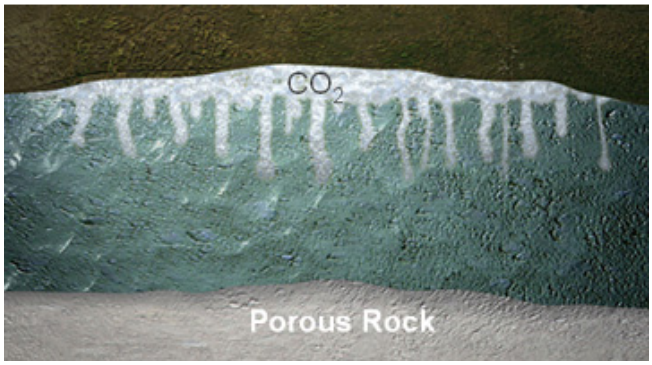

FIGURE 1.4: A sketch of solubility trapping showing how CO_2-brine mixture sink to the bottom (CCP, 2015).

Injecting CO_2 into a deep aquifer, where brine is the main substance inside, due to its gaseous and supercritical state, it is dissolved into this salt water. This process is

known as solubility trapping, since CO_2 is kept thank to the mixture formed. CO_2-brine solute is heavier than just brine, so mixture sinks to the bottom of the formation, trapping the CO_2 more securely.

1.4.3 Mineral trapping

When CO_2 dissolves in water it forms a weak carbonic acid. This weak acid can react with the minerals in the surrounding rock to form solid carbonate minerals. This process could be really slow, depending on the rock, but union between rock and CO_2 is the most permanent and secure form of geological sequestration. Injecting bigger amounts of CO_2 is expected that dissolution could get deeper reservoirs and increase rock surface, consequently, the extent of mineral trapping. But it is important to know that due to changes in concentration, a convective instability can appear. So it is important to find an equilibrium between both.

1.5 Review on literature

This section encompasses previous works and investigations related to dissolution of CO_2 into brine and the impact of chemical reactions. Many works considered the effects of diffusion and convection in many different scenarios. In the following, same results related to convective dissolution will be presented.

1.5.1 Convective dissolution in porous media

Duan & Sun (2003) and Spycher *et al.* (2003) discovered that increasing the temperature, aqueous solubility of CO_2 drops, whereas it increases quickly with pressure rising. These both relationships affects in the results depending on if supercritical conditions in reservoirs are taken. How the point of the investigations is the interaction between brine and CO_2, Portier & Rochelle (2005) and Nomeli *et al.* (2014) used this results to further show that CO_2 solubility depends on brine's salinity, in order to increase the second one, solubility decreases. So as to prevent risk of leakages of supercritical CO_2, convection is really relevant, to increase it, the rate dissolution also increases and therefore time scale over which there is threat of leakages decreases. So it is necessary that time for onset of convection are estimated (Cherezov, 2017). Before convection, diffusion rules the dissolution. Thanks to linear stability analysis, neutral stability curves can be calculated, in any system. Moreover, that curves provide the critical time at which convective instability starts. So many studies present its results of linear stability in terms of dimensionless time for onset of convection (t'_{oc}) and the initial wavelength of convection instability (λ'), characterized as $\lambda' = 2\pi/a'$, where a' is dimensionless wavenumber. The wavelength λ may be also roughly interpreted as the domain width divide by the number of fingers. Therefore, Table 1.5 sum up some investigations with this both parameters.

TABLE 1.5: Summary of linear stability analysis results based on dimensionless parameters in inert systems.

Source	t'_{oc}	λ'
Slim & Ramakrishnan (2010)	48	120
Cheng *et al.* (2012)	48	110
Lindeberg & Wessel-Berg (2011)	49	110
Hassanzadeh *et al.* (2006)	$60 - 130$	130
Ennis-King *et al.* (2005a)	75	95
Xu *et al.* (2006)	75	97
Ennis-King *et al.* (2005b)	78	92
Javaheri *et al.* (2010)	140	140
Riaz *et al.* (2006)	150	90
Chan Kim & Kyun Choi (2012)	170	91

Thanks to the software *Matlab* and the numerical information provided by Table 1.5, we plotted them so as to see if there was any relationship between both parameters, and later use *cftool* command, whose function is find a shape that better approximates the points plotted. Red color point is related to Javaheri *et al.* (2010) values ($\lambda' = 140$, $t'_{oc} = 140$), and it probably shows a mistake, because it is so far from the shape. Then, Figure 1.5 shows the shape of Eq. (1.1), without taking into account this point, which is the best one approximation.

$$\lambda' = 5,119 \cdot 10^7 \cdot (t'_{oc})^{-3,768} + 90,31. \tag{1.1}$$

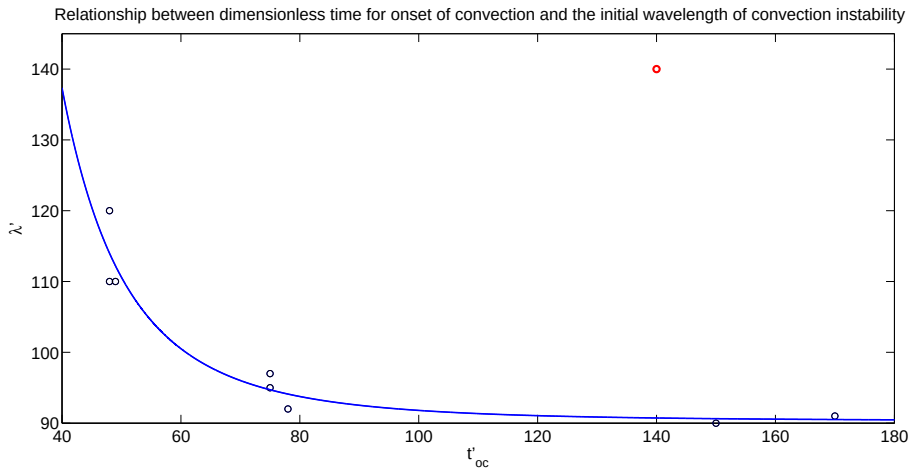

FIGURE 1.5: Approximation of the points shown in Table 1.5 with the purpose of finding a relationship between t'_{oc} and λ'

Some indicators are used in order to check if the interpolation is good. These indicators are Sum of Squares Due to Error (SSE, Eq. (1.2)) and adjusted R-square (adj R-square Eq. (1.4)):

$$\text{SSE} = \sum_{i=1}^{n} w_i \cdot (y_i - \hat{y}_i)^2, \tag{1.2}$$

$$\text{SST} = \sum_{i=1}^{n} w_i \cdot (y_i - \bar{y_i})^2, \tag{1.3}$$

$$\text{adj R-square} = 1 - \frac{\text{SSE}(n-1)}{\text{SST}(\upsilon)}. \tag{1.4}$$

Where $\upsilon = n - m$ is the residual degrees of freedom, n is the number of response values and m is the number of fitted coefficients estimated from the response values. SSE $= 0$ and adj R-square $= 1$ for a perfect interpolation, and how closer values to 0 and 1, respectively, indicates that te model has a smaller random error component, and that the fit will be more useful for prediction.

In this case, Eq. (1.1) found is not exactly good according to the statistical parameters since SSE$= 67,36$ and Adjusted R-square$= 0,8923$. Probably, to accept Eq. (1.1) as the really good one, more experiments should be run.

However, it is not possible estimate the development of the flow once convection has started using only linear stability. Therefore, long-term evolution analysis required numerical simulations (Riaz *et al.*, 2006). So Table 1.6 shows direct numerical simulations results for dimensionless time for onset of convection (t'_{oc}) that many investigators have developed during last 15 years. In order to see this time results from the time at which dissolution flux of CO_2 reaches its minimum.

TABLE 1.6: Summary of numerical simulations based on dimensionless parameter (t'_{oc}) in inert systems.

Source	t'_{oc}
Ghesmat *et al.* (2011)	850
Andres & Cardoso (2011)	1100
Slim (2014)	1200
Pau *et al.* (2010)	1800-3700
Riaz *et al.* (2006)	2000
Hassanzadeh *et al.* (2005)	2300
Farajzadeh *et al.* (2007)	2500
Cheng *et al.* (2012)	3100
Elenius & Johannsen (2012)	4900
Hidalgo & Carrera (2009)	5600

It is significant the difference of order of magnitude between two tables, being

direct numerical simulations grater than linear stability analysis. This is because how each method defines the onset time. Then, while linear stability measures the onset in one point where convection is not still the predominant process, being diffusion which rules the flux, direct numerical simulation measures the onset during transition from diffusive to convective regime. To supercritical CO_2 storage, second one is more relevant. Even so, differences in Table 1.6 are great, and it is depending on which initial amplitude perturbation is used and the analytical approach.

1.5.2 Relevant experimental works

According to Slim & Ramakrishnan (2010), in 2010 they investigated the dissolution of CO_2 considering two idealized configurations, where lower boundary is impermeable, but changing the conditions in the upper boundary. Thus, one is assumed to be impermeable to convective flow whereas the other one is permeable and liquid might move across it. In order to compare different studies made using distinct parameters, Rayleigh number (Ra) is used, which measures the ratio of the strength of convective over diffusive contributions. For the first case, they found that Ra has an important influence on the results, so that for $Ra < 32,50$ instability could be produced. For $32,50 < Ra < 75$, exists a relationship between earliest possible onset time and layer-thickness. Finally, for $Ra > 75$, this time is layer thickness independent. On the other hand, when we talk about permeable boundary, stability diagram is similar, but onset is occurs earlier, and earlier with increasing the layer thickness.

Later, in 2013, the same Slim analyzed the behavior of the dissolution in a almost horizontal Hele Shaw cell, showing in Figure 1.6 the results obtained, where it is possible observed the different regimes as a function of Rayleigh number and advection-diffusion time. Increasing Rayleigh number, obviously, saturation happens later due to a big cell space is provided. This behavior happens until fingers impact the lower boundary, when advection-diffusion is interrupted (Slim *et al.*, 2013). However, this picture has been improved later (Slim, 2014), including the final regime called "shutdown of convection". It was confirmed by numerical investigations of De Paoli *et al.* (2016, 2017) that the regimes are kept in case of anisotropic media.

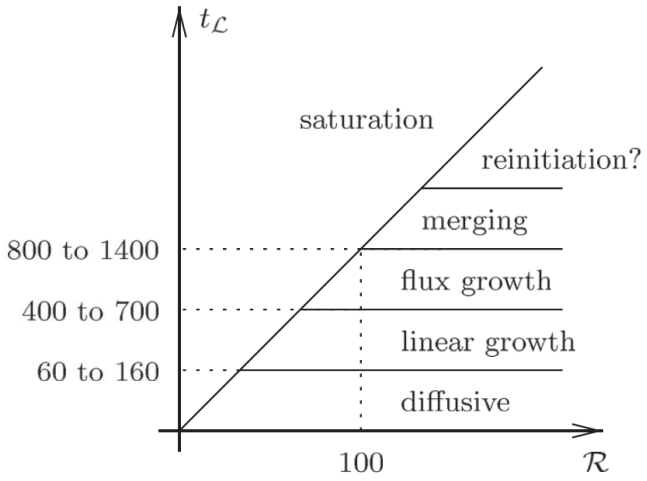

FIGURE 1.6: Summary of different regimes according to Slim *et al.* (2013) studies

Afterwards, Ching *et al.* (2017) studied density-driven convection due to dissolution of CO_2, but in contrast with the previous works, it was focused in high Ra numbers, $2 \cdot 10^4 \leq Ra \leq 8,26 \cdot 10^6$. The results were that for small permeability, that

is, smaller Ra, average wavelengths are similar, whereas heavier fingers were formed for higher permeability. In all this range, large values of total dissolution flux were obtained. Moreover, Nu and Ra have an insignificant dependence.

Chapter 2

Theoretical formulation

As seen in previous sections, the aim of the present experiment is investigate on the brine-CO_2 dissolution process, and to observe how it develops. So, the study starts from first contact between water and powder up to the complete dissolution. However, there is a big disadvantage if we compare the real experiment with what really happens: geological conditions. Temperature 1 km beneath the surface of the Earth could be 25-30^{o}C greater than atmospheric conditions (it is possible get it in a laboratory), but pressure could be greater than 100 bar (Ching *et al.*, 2017), and it is not as easy to acquire. So mimic underground conditions is truly hard. Moreover, use carbon dioxide as solute complicates the test because it must be captured and sequestrated from some thermal process, wasting a considerable amount of energy for a simple experiment. To fix these disadvantages, potassium permanganate ($KMnO_4$) powder will be used instead of CO_2, and re-ionized water will replace brine (similar density between both kinds of water). The resulting density increased ($\Delta\rho = 46$ kg m^{-3} at 25^{o}C (Novotny & Sohnel, 1988)) and saturated mass fraction of $KMnO_4$ to water ($\omega_{sat} = 0,067$) were comparable to the mixing condition of CO_2 into brine ($\Delta\rho = 30$ kg m^{-3} and $\omega_{sat} = 0,07$ at reservoir conditions) (Garcia, 2003). Similar to change of the liquid density for CO_2 dissolved in saline, $\Delta\rho$ linearly increased with the dissolution concentration (Ching *et al.*, 2017) and concentration is

$$C_w = \rho(w)w \qquad (\text{kg/m}^3), \tag{2.1}$$

where $\rho(w)$ is mixture density (kg/m^3) and ω is the mass fraction of solute to the solution.

To compare the data obtained running different experiments, dimensionless parameter is required to contrast the values and extract a conclusion. This parameter will be Rayleigh (Ra) number.

$$Ra = \frac{HK\Delta\rho g}{\phi D\mu}, \tag{2.2}$$

where H is the cell height, K is the effective permeability, $\Delta\rho = \rho_{max} - \rho_0$ is the maximal density difference between the saturated mixture and the original solution, g is the acceleration due to gravity, $\phi = 1$ is the effective porosity, D is diffusivity and μ is dynamic viscosity. Of these, $\Delta\rho, \phi, D, \mu$ depend on the materials, so we can not change its value and will be the same in all experiments. g is a constant that neither could be change. Therefore, only H and K could be changed in order to modify Ra number. However, all the experiments will be run in the same cell, and then H will be, again, a fix value. We conclude that in our test, $Ra \propto K$, where $K = b^2/12$. b is the distance between two plates, and separating or getting the polycarbonates closer is our way to change the Ra number.

The contact between water and the mineral ($KMnO_4$) gives a purple colour to the

mixture and depending on the colour intensity is possible determine the concentration in each point. In order to get it, pictures will be taken regularly to register the mixture development since the onset to total dissolution. Afterwards these pictures will be treat with *Matlab* software to apply a numeric value to each point in the photo, and reconstruct the concentration of $KMnO_4$. The procedure followed is: after taking the photos, intensity pixel could be read. Subsequently, background and backlightning panel corrections are applied, getting then a good value of intensity. Later, reading this intensity, mass fraction is known, and after that, thank to had found before the relationship between intensity and concentration, this is calculated. This procedure is explain in detail in Section 2.1 and Chapter 5. The final goal will be to calculate the flux (F [(kg/m^3)/m]), according to:

$$F(\mathrm{t}) = \frac{1}{L} \int \left. \frac{dC}{dz} \right|_{z=0} dx. \tag{2.3}$$

One of the challenges in the present experiment is that boundary conditions could not be easily kept. But we could know the concentration, as we explained before thank to the mixture calibration. Then, once we know the concentration $C(x, z)$ in each pixel we can calculate for each time the whole amount of solute dissolved (M [kg]).

$$M = b \cdot (bHL) \cdot \int_0^h \int_0^L C(x, z) dx dz, \tag{2.4}$$

$$M = b \cdot (bHL) \cdot \frac{\sum_{i=0}^{n_x} \sum_{j=0}^{n_z} C^*(i, j)}{n_x n_z}, \tag{2.5}$$

where n_x are the pixels in X-axis (cell length) and n_z are the pixels in Y-axis (cell height) and C^* is the concentration in each pixel. After applying it,

$$F(\mathrm{t}) = \frac{1}{b^2 LH} \frac{dM}{dt}. \tag{2.6}$$

Anyway, in Figure 2.1 a sketch of the procedure followed in order to get the flux is shown, where inside each box is written the next step done with respect to the previous function.

TABLE 2.1: Constants values for $KMnO_4$ substance

A	B	C	D	E	F
$1.223/10^{-2}$	$-1.029/10$	$8.093/10^3$	-14.85	$90.79/10^2$	$-75.66/10^4$

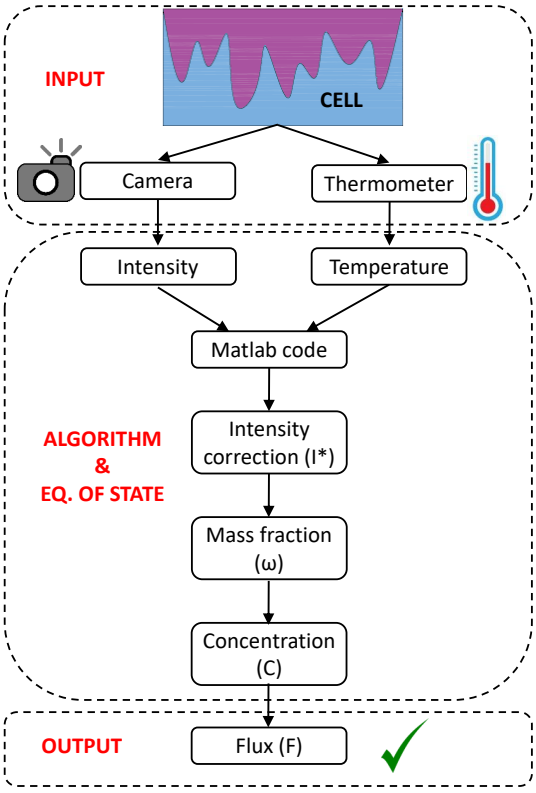

FIGURE 2.1: Scheme of the procedure followed to obtain flux value

2.1 Relationship between concentration and density

In previous sections we observed that the concentration of a mixture depends on mass fraction (ω) and density, which is also a function of the mass fraction ($\rho(\omega)$). So in this point we are going to explain the relationship between concentration and density, because it is not trivial find its value.

If we consider water, its density only depends on the temperature, whereas if we talk about a substance that is dissolved in water, the density depends on temperature and also on the concentration (Novotny & Sohnel, 1988),

$$\rho = \rho_{water} + Ac + Bct + Cct^2 + Dc^{3/2} + Ec^{3/2}t + Fc^{3/2}t^2, \tag{2.7}$$

where A through F are constants that depend on the substance mixed with water (Table 2.1), c is the solute concentration (mol/dm^3), t is the temperature (^{o}C) and ρ is density (kg/m^3). In the case of study, solute is $KMnO_4$ and its constants are:

But in Eq. (2.11) we also see that we need to know ρ_{water}, whose formula is

$$\rho_{water} = 999,65 + 2,0438 \cdot 10^{-1}t - 6,174 \cdot 10^{-2}t^{3/2}. \tag{2.8}$$

Then, if t is known, it is possible calculate ρ_{water}, therefore ρ will only depend on concentration. We also know that $c_\omega = \rho(\omega)\omega$, written before. But a conversion of units is needed because in this second formula, c_ω is expressed as (kg/m^3) and not as mol/dm^3. $KMnO_4$ molar mass is 158,034 g/mol. Applying the conversion of units:

$$\frac{1\text{mol}}{\text{dm}^3} = \frac{1\text{mol}}{\text{dm}^3} \cdot \frac{158,034\text{g}}{\text{mol}} \cdot \frac{\text{kg}}{1000\text{g}} \cdot \frac{1000\text{dm}^3}{\text{m}^3} = \frac{158,034\text{kg}}{\text{m}^3}. \tag{2.9}$$

To visualize easier the relationship of units,

$$c^*[mol/dm^3] = \text{MM} \cdot c[kg/m^3]. \tag{2.10}$$

Now we have an equation system of 2 equations with 2 unknown quantities. In order to find the concentration, some mathematics calculations have been done, to visualize better the procedure and the final results:

$$\rho = \rho_{water} + c^* \cdot (A + Bt + Ct^2) + c^{*3/2} \cdot (D + Et + Ft^2), \tag{2.11}$$

$$\rho = \rho_{water} + c^*\alpha + c^{*3/2}\beta, \tag{2.12}$$

where

$$\alpha = A + Bt + Ct^2 \qquad \beta = D + Et + Ft^2. \tag{2.13}$$

Substituting Eq. (2.13) in the another equation, we obtain:

$$c = [\rho_{water} + c^*\alpha + c^{3/2}\beta] \cdot \omega. \tag{2.14}$$

We use Eq. (2.10) first:

$$c^* \cdot \text{MM} = [\rho_{water} + c^*\alpha + c^{*3/2}\beta] \cdot \omega, \tag{2.15}$$

and we develop Eq. (2.15) to obtain:

$$c^{*3/2} = \epsilon - \delta \cdot c^*, \tag{2.16}$$

where,

$$\epsilon = -\frac{\rho_{water}}{\beta} \qquad \delta = -\frac{1 - \alpha\gamma}{\beta\gamma} \qquad \gamma = \frac{\omega}{\text{MM}}. \tag{2.17}$$

Eq. (2.16) is a non linear equation, and an analytical solution is not available. Therefore, it has to be solved numerically, which means that we guess an initial value of c, we calculate $c^{3/2}$ and afterwards we solve c from Eq. (2.16),

$$c^* = \frac{c^{*3/2} - \epsilon}{-\delta}. \tag{2.18}$$

And then, if the new value is equal to the value that we assumed, we have found the solution. If do not, we apply again Eq. (2.18) with the new value of c, and we follow the same procedure until both c are equal, or until the difference between both is small enough. Before doing it analytically, we plotted the relationship between water density and temperature, solution density and solute concentration and concentration with density solution and density water difference, shown in Figure 2.2. In order to get the two graphics that are at the right side, a temperature has to be assumed. In our case, we established that $t = 25^oC$. It is observed that temperature does not have a big influence on water density (with a difference of 40^oC the maximum difference of density is around 10 kg/m^3) and there is more influence of concentration in solution

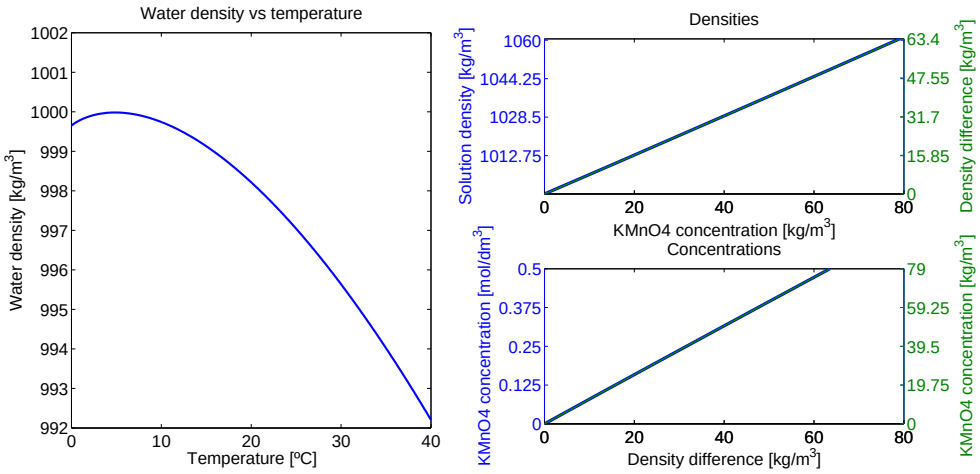

FIGURE 2.2: Relationship between temperature, water density, solution density and concentration

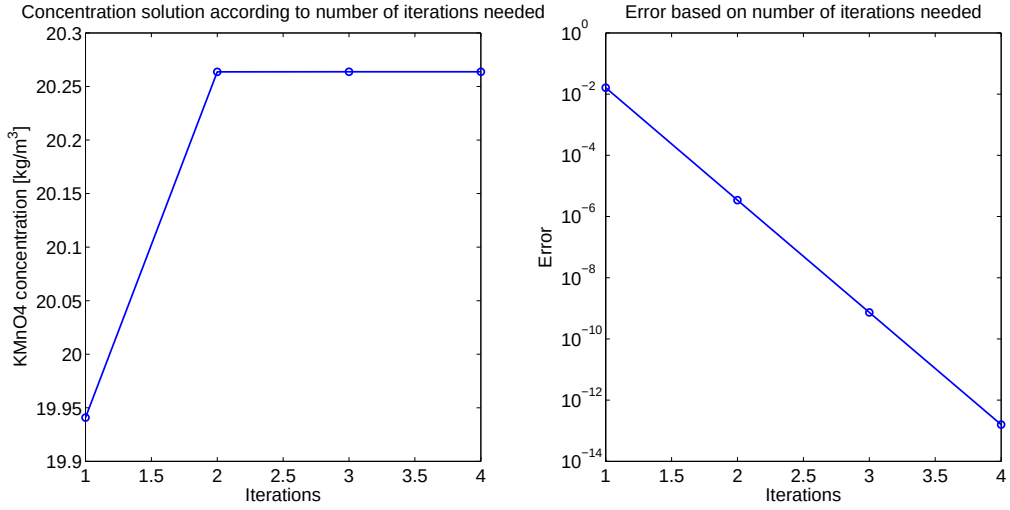

FIGURE 2.3: Number of iterations needed to solve Eq. (2.16)

density, but still is not large (adding 80 kg/m^3 of $KMnO_4$, density increases up to $6,37$ %).

Provided the small influence of concentration in density, we assume that the first value of concentration to start iteration (c_0) will be $c_0 = \rho(\omega_0)\omega$, where ω_0 is the density at the beginning, when there is no solute yet, that is, only water.

A first verification was done in order to validate the *Matlab* code. We assumed that $t = 25^oC$, $\omega = 0,02$ and error $= 1E-11$, where error is calculated as error $= (c^{n-1} - c^n)/(c^{n-1})$. The results are shown in Figure 2.3. Y axis at right figure is plotted in logarithmic scale. The concentration to the mass fraction done is $20,2637$ kg/m^3 and the error is $1,58E-13$. We observed that 4 iterations were needed to find c.

Once seen that the program works, the procedure was the following: we applied the code to 100 values of ω between 0 and $0,1$, and then we found the relationship between concentration and mass fraction, first graphically and later finding the equation that relates both. Thus, when we knew mass fraction thanks to pictures analysis during mixture calibration, we could calculate concentration.

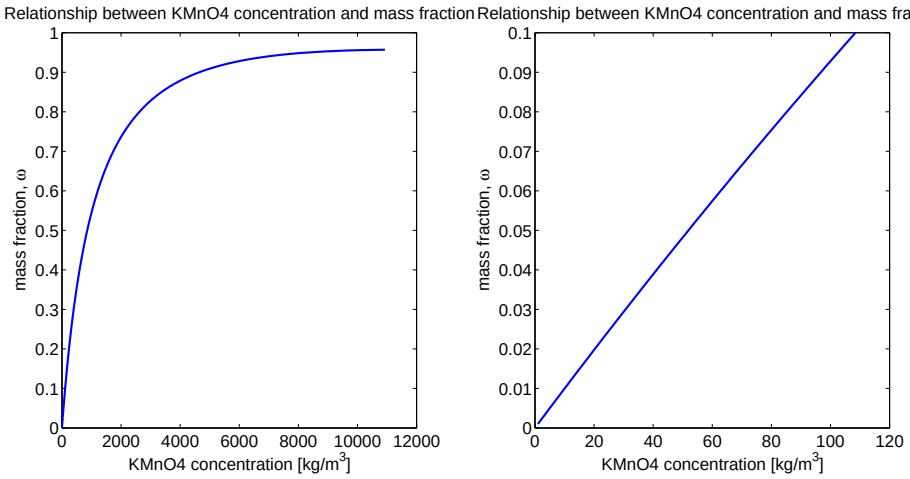

FIGURE 2.4: Relationship between mass fraction and $KMnO_4$ concentration, showing that the first part is almost linear

If we study Figure 2.4, the shape of the plot placed at left, at the beginning the slope is pronounced whereas when the value of ω reaches $0,6$ the slope decreases until at $\omega = 0,9$ is almost flat. Obviously, mass fraction in a system with dissolution never can be 1, which means that only there is one substance. However, we are going to work with mass fraction between 0 and $0,1$, so at right is plotted a zoom of the total curve, but only between that values. And it is possible to observe that relationship between mass fraction and the $KMnO_4$ concentration is linear. If we work with the software *Matlab*, we could find the function that approximates the curve. For the complete plot (left), we could approximate it with a sixth degree polynomial (Eq. (2.19)), where a,b,c... are constants whose value are shown in Table 2.2 and x means $KMnO_4$ concentration. But, since we work with values between 0 and $0,1$, we could approximate the relationship to a linear equation (Eq. (2.20)) found, again, with *Matlab*.

$$\omega = ax^6 + bx^5 + cx^4 + dx^3 + ex^2 + fx + g. \tag{2.19}$$

TABLE 2.2: Constants values for Eq. (2.19)

a	**b**	**c**	**d**	**e**	**f**	**g**
$9,884$	$2,675$	$-2,871$	$1,578$	$-4,864$	$8,941$	$8,289$
$\text{x}10^{-23}$	$\text{x}10^{-18}$	$\text{x}10^{-14}$	$\text{x}10^{-10}$	$\text{x}10^{-7}$	$\text{x}10^{-4}$	$\text{x}10^{-3}$

$$\omega = 0,0009216x + 0,001434. \tag{2.20}$$

However, a problem appears if we evaluate Eq. (2.20), and this is when concentration is 0 ($x = 0$) mass fraction should be 0 too, but it is 0,001434. And it means that, when we have a $\omega < 0,001434$ (because we find concentration from ω), then concentration would be negative, and it is not physically possible. To fix it, we use a second polynomial equation, and its shape is:

$$\omega = -7,183 \cdot 10^{-7}x^2 + 0,0009994x + 3,242 \cdot 10^{-5}. \tag{2.21}$$

With this new equation, that it is almost linear because the quadratic coefficient is close to 0, the shape goes through the origin if we assume $3,242 \cdot 10^{-5} \simeq 0$. And finally, we only will have concentration values smaller than 0 when $\omega < 3,242 \cdot 10^{-5}$, but it is a value really small and we are not going to work with so small. Finally, how we find concentration (C) from mass fraction, and not backwards, we solve Eq. (2.21) to isolate concentration:

$$C = 917,3\omega^2 + 991,9\omega + 0,04512. \tag{2.22}$$

Chapter 3

Error theory

When a measurement is done, we will always have some errors. Sometimes, the effect of these errors can be neglected, but sometimes it does not, so these errors have to be taken into account. And it is important to estimate the experimental error, known as uncertainty. This error depends on the devices used in order to measure what we need. And now, the theoretical formulation is explained and applied to the different formulas that we are going to use throughout this work.

Suppose we have a function (U) that depends on many variables, that we are going to call A, B, C, etc. Each variable is associated to an independent quantity, measured before. Then, we can represent $U = f(A, B, C...)$. For each variable, we have to assume an uncertainty, measurable a lot of times with the device tolerance. We represent this tolerance as $\Delta A, \Delta B, \Delta C...$ Once we have measured each variable ($\bar{A}, \bar{B}, \bar{C}...$), we apply the equation, substituting the expectation values and obtaining a result, called $\bar{U}$.

$$\bar{U} = f(\bar{A}, \bar{B}, \bar{C}...). \tag{3.1}$$

But when we take into account the error, the value is not presented as a number but an interval, which means that considering the error of the devices, the exact value is contained in this interval. So it is necessary to calculate the uncertainty for U (Scuro, 2004), and it is given by

$$\Delta U = \sqrt{\left(\frac{\partial U}{\partial A}\right)^2 (\Delta A)^2 + \left(\frac{\partial U}{\partial B}\right)^2 (\Delta B)^2 + \left(\frac{\partial U}{\partial C}\right)^2 (\Delta C)^2 + ...}, \tag{3.2}$$

where $\bar{A}, \bar{B}, \bar{C}$ are used when partial derivatives are calculated theoretically. So, the appropriated final value of U is

$$U = \bar{U} \pm \Delta U. \tag{3.3}$$

3.1 Mass fraction error

In order to conduct the calibration of the mixture, how it will be explained later in other section, it is necessary find experimentally the relationship between mass fraction and light intensity, and some mixtures are needed, each one with a different mass fraction. So it is necessary calculate this value that indicates the concentration. The mass fraction relate the solute mass with total mass of the mixture.

$$w = \frac{m_{solute}}{m_{solute} + m_{solvent}}, \tag{3.4}$$

where in our case solute is $KMnO_4$ whereas water is our solvent. To determine both values, obviously, it is necessary to use a scale to weight both quantities, and we will have some of the error above mentioned. So it is required to apply Eq. (3.3)

to Eq. (3.4). In this case, the formula depends on 2 variables, and these variables are measured with the same device, so ΔA and ΔB is equal, and its value is $0,001$, because the scale tolerance is $0,001$ g and mass values are in gramms. If we apply Eq. (3.2) to Eq. (3.4), the derivatives are:

$$\frac{\partial \omega}{\partial m_{solute}} = \frac{m_{solvent}}{(m_{solute} + m_{solvent})^2}, \tag{3.5}$$

$$\left(\frac{\partial \omega}{\partial m_{solute}}\right)^2 = \frac{m_{solvent}^2}{(m_{solute} + m_{solvent})^4}, \tag{3.6}$$

$$\frac{\partial \omega}{\partial m_{solvent}} = \frac{-m_{solute}}{(m_{solute} + m_{solvent})^2}, \tag{3.7}$$

$$\left(\frac{\partial \omega}{\partial m_{solute}}\right)^2 = \frac{m_{solute}^2}{(m_{solute} + m_{solvent})^4}. \tag{3.8}$$

Once we have all the derivatives calculated, we substitute Eq. (3.6) and Eq. (3.8) on Eq. (3.2), and the result is

$$\Delta\omega = \sqrt{\frac{m_{solvent}^2}{(m_{solute} + m_{solvent})^4}(\Delta A)^2 + \frac{m_{solute}^2}{(m_{solute} + m_{solvent})^4}(\Delta B)^2}. \tag{3.9}$$

If we join common terms in Eq. (3.9), and knowing that $\Delta A = \Delta B = \Delta m_{solute}$, then

$$\Delta\omega = \sqrt{\frac{m_{solute}^2 + m_{solvent}^2}{(m_{solute} + m_{solvent})^4}(\Delta m_{solute})^2}. \tag{3.10}$$

So now, we only have to substitute the numerical values for theoretically values for each mixture with different concentration. The table with this values is shown in the Chapter 5

3.2 Rayleigh number error

Another formula that will be used is Rayleigh number, in order to compare different experiments with a dimensionless number. How some terms are measured by us, as for example distances, it is necessary apply error theory to Eq. (2.2). The variables that bring with error are H and K. Therefore, like it has been done before, we have to calculate the derivatives with respect to this variables. Reminding that we do not measure directly the effective permeability but the gap between both plates (b), and then $K = b^2/12$. Then, to calculate the derivative with respect to b, first we have to substitute it on Ra formula.

$$\frac{\partial Ra}{\partial H} = \frac{K\Delta\rho g}{\phi D\mu} = \frac{b^2\Delta\rho g}{12\phi D\mu}, \tag{3.11}$$

$$\frac{\partial Ra}{\partial b} = \frac{Hb\Delta\rho g}{6\phi D\mu}. \tag{3.12}$$

Substituting Eq. (3.11) and Eq. (3.12) on Eq. (3.2),

$$\Delta Ra = \sqrt{\left(\frac{b\Delta\rho g}{\phi D\mu}\right)^2 \cdot \left(\frac{b^2(\Delta b)^2}{12^2} + \frac{H^2(\Delta H)^2}{6^2}\right)}. \tag{3.13}$$

How b has the precision of the shims and H is measured with calipers, it is not possible to simplify Eq. 3.13.

For the parameters of Eq. (2.2), how it has been said, only b changes. And we also assume that all error's parameters, except H and K, are equal to 0. In order to assume that $\Delta\omega = 0$, some retouches are required in the typical formula, depending on the latitude (phi) and the height (h) relative to sea level of the laboratory. Then, $g = \text{IGF} + \text{FAC}$, where IGF is International Gravity Formula (Eq. (3.14)) and FAC is Free Air Correction (Eq. (3.15)).

$$\text{IGF} = 9,780327 \cdot (1 + 0,0053024 \cdot (\sin \cdot(\text{phi}^2) - 0,0000058 \cdot \sin \cdot(2 \cdot \text{phi}^2), \tag{3.14}$$

$$\text{FAC} = -3,086 \cdot 10^{-6} \cdot h, \tag{3.15}$$

where in our case, $h = 203$ m, since the height is 194 m + 9 m that represents 2 floors of 4,5m each one and $phi = 48,179246 \cdot \pi/180$.

Applying these two formulas, $g = 9,8084$ m/s^2. The rest of the parameters values used in Eq. (2.2) are shown in Table 3.1.

TABLE 3.1: Values of the parameters used in Rayleigh formula. D is extracted of (Ching *et al.*, 2017) and the viscosity is at 25 °C.

g [m/s^2]	$\Delta\rho$ [kg/m^3]	H [m^2]	ϕ [-]	D [m^2/s]	μ [kg/s· m]
$9,8084$	30	$70,6 \cdot 10^{-3}$	1	$1,65 \cdot 10^{-9}$	$8,91 \cdot 10^{-4}$

Table 3.1 shows all variables except the effective permeability (K) due to it enables to change Ra number. Its numerical values are shown in Table 3.3 where it is displayed the value of the gap (b), the permeability (K), the Rayleigh number (Ra), its error according to Eq. (3.13) (ΔRa) and the % difference ($\Delta Ra\%$). In our case, then, the tolerances are $\Delta b = 10^{-4}$ mm whereas $\Delta H = 2^{-5}$ mm.

TABLE 3.2: Values of parameter b such as Ra and its tolerance for the experiments that should be run.

b [m]	K [m^2]	Ra [-]	ΔRa [-]	$\Delta Ra\%$ [-]
$1 \cdot 10^{-4}$	$8,33 \cdot 10^{-10}$	$1,18 \cdot 10^{4}$	$4,71 \cdot 10^{3}$	$40,0$
$2 \cdot 10^{-4}$	$3,33 \cdot 10^{-9}$	$4,71 \cdot 10^{4}$	$9,42 \cdot 10^{3}$	$20,0$
$3 \cdot 10^{-4}$	$7,50 \cdot 10^{-9}$	$1,06 \cdot 10^{5}$	$1,41 \cdot 10^{4}$	$13,3$
$4 \cdot 10^{-4}$	$1,33 \cdot 10^{-8}$	$1,88 \cdot 10^{5}$	$1,88 \cdot 10^{4}$	$10,0$
$5 \cdot 10^{-4}$	$2,08 \cdot 10^{-8}$	$2,94 \cdot 10^{5}$	$2,36 \cdot 10^{4}$	$8,0$
$6 \cdot 10^{-4}$	$3,00 \cdot 10^{-8}$	$2,94 \cdot 10^{5}$	$2,83 \cdot 10^{4}$	$6,7$
$7 \cdot 10^{-4}$	$4,08 \cdot 10^{-8}$	$5,77 \cdot 10^{5}$	$3,30 \cdot 10^{4}$	$5,7$
$8 \cdot 10^{-4}$	$5,33 \cdot 10^{-8}$	$7,54 \cdot 10^{5}$	$3,77 \cdot 10^{4}$	$5,0$
$9 \cdot 10^{-4}$	$6,75 \cdot 10^{-8}$	$9,54 \cdot 10^{5}$	$4,24 \cdot 10^{4}$	$4,5$
$10 \cdot 10^{-4}$	$8,33 \cdot 10^{-8}$	$1,18 \cdot 10^{6}$	$4,71 \cdot 10^{4}$	$4,0$

TABLE 3.3: Values of parameter b such as Ra and its tolerance for the experiments that should be run.

b x10^{-4} [m]	K x10^{-8} [$\mathbf{m}^2$]	Ra x10^5 [-]	ΔRa x10^4 [-]	$\Delta Ra\%$ [-]
1	0,0833	0,118	0,471	40,0
2	0,333	0,471	0,942	20,0
3	0,750	1,06	1,41	13,3
4	1,33	1,88	1,88	10,0
5	2,08	2,94	2,36	8,0
6	3,00	2,94	2,83	6,7
7	4,08	5,77	3,30	5,7
8	5,33	7,54	3,77	5,0
9	6,75	9,54	4,24	4,5
10	8,33	11,8	4,71	4,0

Thanks to Table 3.3 is visible that $1,18 \cdot 10^4 < Ra < 1,18 \cdot 10^6$, being this the interval of operation for our experiments in order to compare results.

Chapter 4

Light calibration

The brightness along the whole panel is not exactly the same due to metal frame influence, reflection, etc. so images must be corrected. We define this process as "Light calibration".

4.1 Backlighting panel calibration

Once we got the backlighting panel, the first step was calibrated it thank to running some experiment. Dimension's panel were 190x100mm, whereas the effective cell measures were 141x78,6mm, how it is shown in Figure 6.1. It was also possible change the brightness modifying the voltage applied, from 0 to 5 V, corresponding 5 V to the most bright situation. The aim of the experiment was to verify bright smoothness in the whole panel, or at least in the pictures taken, to avoid disturb the results. In order to do it, the stuff required consisted in: the backlighting panel, a voltmeter to measure the voltage supplied to the panel, a bracket to hold the Hele-Shaw cell and avoid hold it on the table surface in order to avoid getting disturbed results, a black craft paper slice to put on the table and avoid reflexion of his white surface, a camera and the own cell, with the devices associated to the experiment. In Figure 6.2 is shown a simplified sketch, with the respective lengths between the objects.

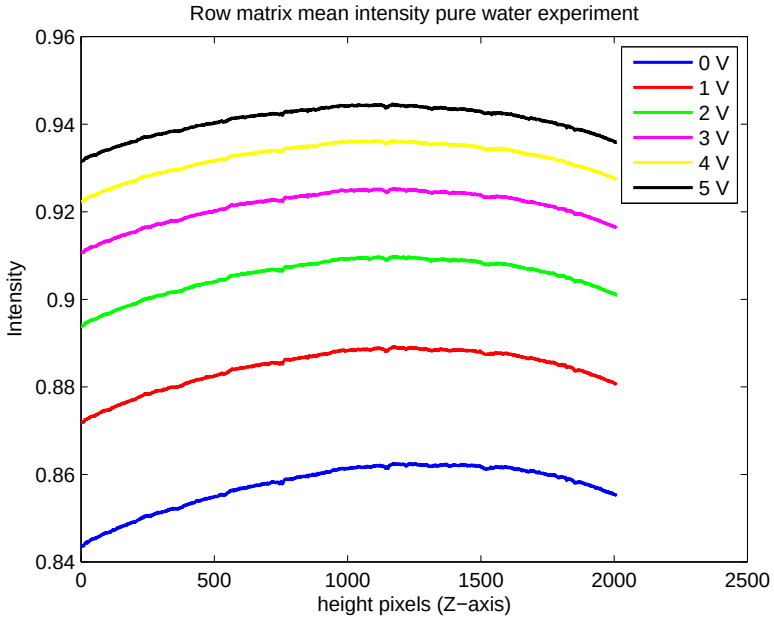

FIGURE 4.1: Row matrix mean intensity in pure water experiment

Once located all the devices in its position, 6 photos were taken, only changing the voltage supplied between each one, being 0, 1, 2, 3, 4 and 5 V respectively. This procedure was run twice: the first one was done with just pure water inside the Hele-Shaw cell, whereas in the second one, the cell was filled with $KMnO_4$-water solution. The mixture was prepared before, well-mixed and left for a while, to ensure that the concentration was the same in all the liquid. Afterwards, the pictures taken were analysed with *Matlab*. In the same way that we worked the case before, the results that we wanted to obtain were the average concentration in all the cell (we were working with a mixture prepared, so all the liquid had to have the same concentration) to evaluate the influence of the bright in the results comparing the 6 pictures, and find if the light is the same in all the photo for each experiment, or if on the contrary, the images suffered from uneven lighting. The image is corrected in the way that for each dz in the image Eq. (4.1) is applied.

$$I = \frac{1}{L}\int_0^L I(x,z)dx. \tag{4.1}$$

The results obtained are shown in Figure 4.1 and Figure 4.2. It is observed that the shape of the 6 curves are almost totally equal, but are a bit different if we compared both experiments. It was also appreciated that the grater the voltage, the most together curves were. And it is important to remind that when *Matlab* reads a grey image, i.g. a matrix, 0 represents black colour and 1 represents white colour. That is the point why the values are so big. Then, it is shown that the grater the voltage, the grater the brightness. Moreover, using the images taken to the mixture (Figure 4.3), it is also visible the light intensity difference between both. This difference is related to the distance between blue and black lines in Figure 4.2. And it is shown using mixture experiment because the difference is more visible than using only pure water.

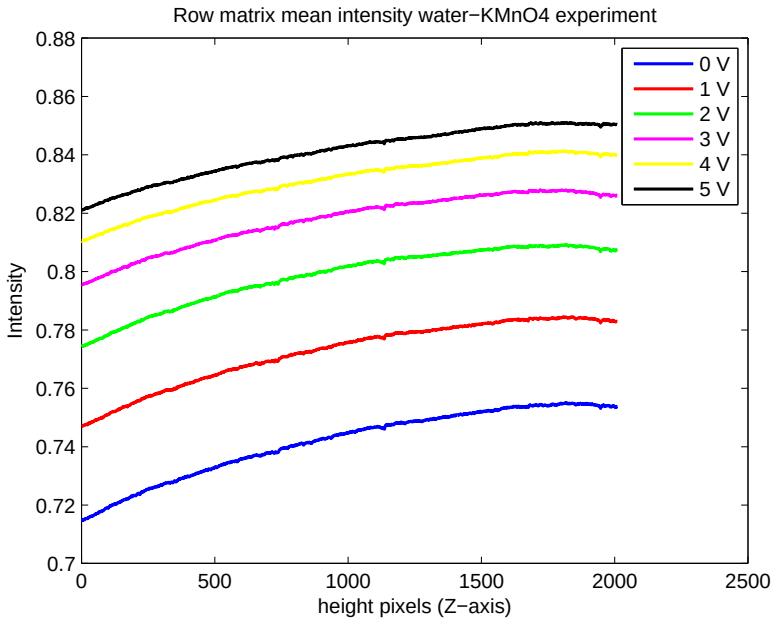

FIGURE 4.2: Row matrix mean intensity mixture experiment

Summing up, pure water shapes are what we expected, a parabolic shape, because we knew that the recorded images suffered from uneven lighting, with the centre of cell being brighter than the edges, according to other thesis (Cherezov, 2017). In order to

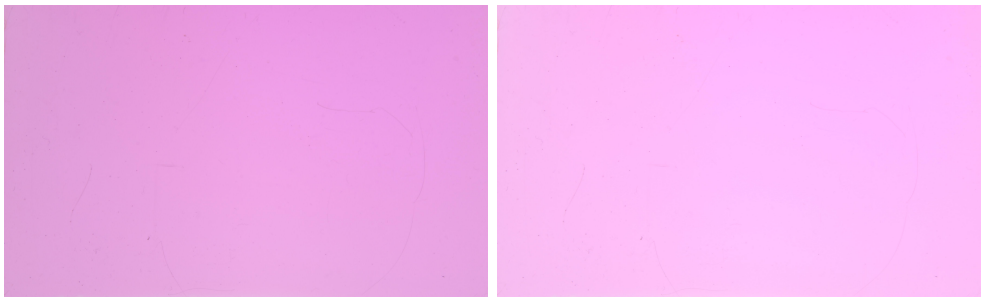

(a) Original image when voltage is 0V. (b) Original image when voltage is 5V.

FIGURE 4.3: Comparison of two images with same $KMnO_4$ concentration, but injecting different voltage.

fix it, background correction will be explain in detail below. However, water-$KMnO_4$ curves don't show what we expected, increasing all time, and being the bottom part much brighter than upper or central part, when it should be symmetric. It is due to unavoidable reflections.

And how it is said before, image (or matrix in *Matlab*) average intensity has been also calculated. We wanted to check how values changed depending on the voltage supplied to the panel. Table 4.1 and Table 4.2 show intensity results got, such as the exact voltage values, with 1 mV precision.

TABLE 4.1: Summary values of light calibration using pure water

	Pure water					
	0 V	**1,001 V**	**2 V**	**2,999V**	**4 V**	**5V**
Mean	0,8575	0,8844	0,9054	0,9211	0,9323	0,9408
Difference	-	0,0269	0,0210	0,0157	0,0112	0,0085

TABLE 4.2: Summary values of light calibration using water-$KMnO_4$ mixture

	Water-$KMnO_4$ mixture					
	0 V	**0,999 V**	**2 V**	**3,002V**	**3,999 V**	**5V**
Mean	0,7416	0,7724	0,7985	0,8176	0,8310	0,8409
Difference	-	0,0308	0,0261	0,0191	0,0134	0,0099

Summarizing Table 4.1 and Table 4.2 information, averaged intensity rises up while voltage increases, but its influence is less significant when grater is it, how we can see in the row "Difference", whose value is intensity mean minus the intensity before (e.g. $0,7724 - 0,7416 = 0,031$). Then, voltage used during the experiment should be between 3 and 5 V.

4.2 Background correction: common procedure

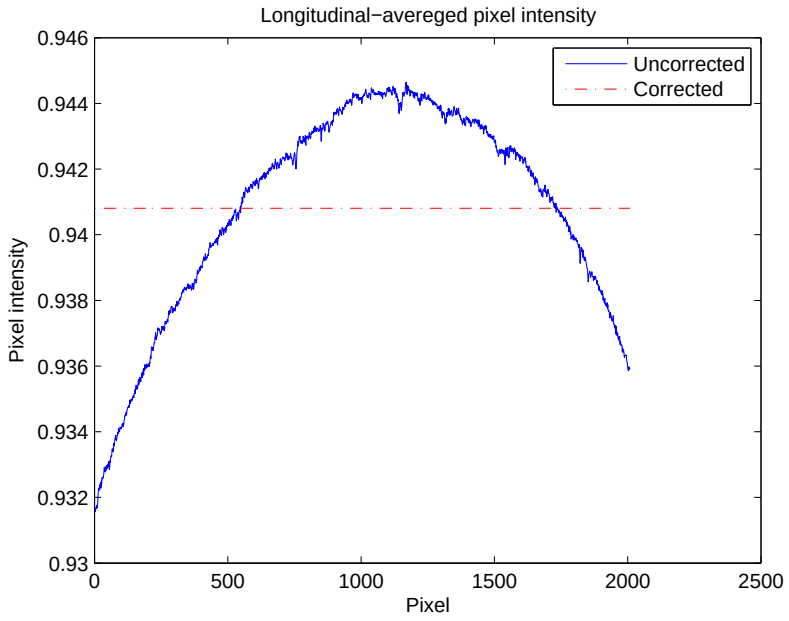

FIGURE 4.4: Longitudinal-averaged pixel intensity along a vertical transect

As above mentioned, due to pictures suffered from uneven lighting, and the centre is brighter than the edges, background correction is needed. Following the procedure followed by Cherezov (2017), we take the water-$KMnO_4$ mixture picture and pure water image, both using the same voltage. Pure water image acts as reference and captures the distribution and unevenness of the light illuminating the cell. Then, the image is normalised by dividing each image pixel (Pixel $_{\text{original}}$) by the corresponding pixel value of the reference image of a pure water cell (Pixel $_{\text{reference}}$) and then multiplying by the average pixel intensity, shown in Figure 4.4.

$$\text{Pixel}_{\text{corrected}} = \frac{\text{Pixel}_{\text{original}}}{\text{Pixel}_{\text{reference}}} \cdot \text{average}_{\text{pixel intensity}} \tag{4.2}$$

Although the procedure before had been applied, any noise could remain. In order to avoid it, or at least, reduce it, a median smoothing filter could be applied. It consists in take a 3 x 3 pixel square, calculate the average of these 9 pixels intensity and replace this new value for the 9 pixels. Obviously, then matrix will be reduced to a third dimension, as rows such as columns. But although both matrix have different dimension, they could be compared each other. To compare it, it is necessary rescale X-axis. In Figure 4.2 X-axis represents pixels, but we want that distance be X-axis. And the distance chosen is the image real length, that is, what is the length of the image part taken, in mm. In this way, both graphics will have same scale and could be compared. In order to get it on *Matlab*, first of all, we measure the length (90 mm in own case), afterwards we create a step: h_i = length / (size (matrix_i, 1) -1), $i = 1, 2$, where 1 means related to original matrix and 2 to corrected matrix. Then, the X vector will be $x_i = 0 : h_i :$ length and finally we only have to plot (x_i, y_i), where y represents pixel intensity matrix. Such as it is shown in Figure 4.5, it is difficult to appreciate the difference between both curvatures in the whole image, but if we

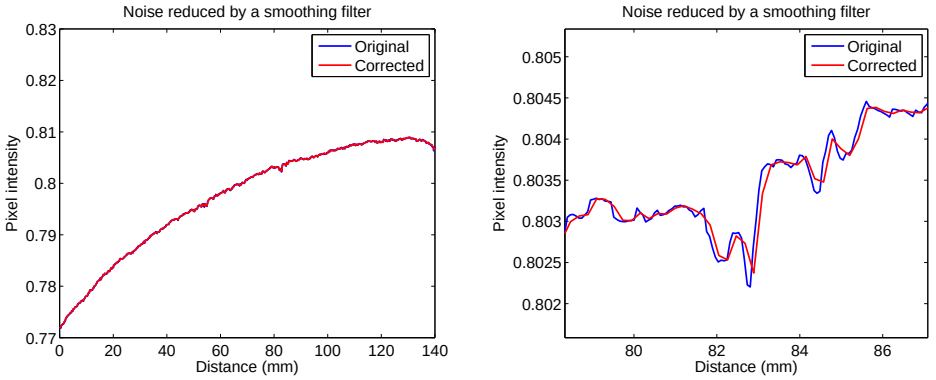

(a) Total cell distance.

(b) Image increased in order to appreciate the difference.

FIGURE 4.5: Curvatures comparison before and after applying a smoothing filter.

zoom in some part, we could check how red line corrects blue line noise. However, this procedure has a disadvantage: the effective resolution decreases as well as the amount of information that are locally available. Moreover, the light intensity is also function of the mass fraction, and not only of the position. Therefore a more sophisticated system is required to calibrate the cell, and will be presented in Section 5.5.

Chapter 5

Mixture calibration

In order to calculate $KMnO_4$ concentration, mass fraction should be calculated before. After images acquisition, pixel intensity is known. However, to convert these values to concentration, mixture calibration must be performed, and we need to find the relationship between the intensities and ω. And this procedure has to be done independent of and before of the real experiment. So in next subsections the procedure and the results achieved are explained.

5.1 First sampling

The aim of the experiment was find the relationship between mass fraction (ω) and the mixture light intensity, obtained by taking photos of this mixture and analysing it afterwards. Thus, we wanted to plot it, and Y-axis represented mass fraction, whose formula is $\omega = m_{sol}/m_{tot}$, whereas X-axis represented the intensity, in a non-dimensional way. In order to get it, it is plotted the ratio between mixture intensity and intensity with pure water (formula Intensity/Intensity with pure water). To obtain accurate results, the experiments had to be done in a Hele-Shaw cell. Nevertheless, so much time was required because in each experiment the cell had to be assembled, run the test and afterwards disassemble in order to remove the fluid.

FIGURE 5.1: Test tube where mixture calibration was supposed to do in.

Therefore, we wanted to use a test tube where to add the dissolution and take there the pictures. The set of instruments required was based in a scale with a $0,001$ g precision to weigh the water and the $KMnO_4$powder, these both substances to prepare the mixture and the test tube. The initial idea was weigh both matters and mixed afterwards in a vase until getting a well-mixed fluid, with uniform concentration in whole dissolution. But one of the problems that we have to deal with was that the test tube hasn't have an uniform shape, but the bottom part was wider that the upper part, with a cylinder shape, as it is shown in Figure 5.1. And then we noticed that

in the base the colour was darker because of more fluid was contained, although the concentration was exactly the same. So the values that we would get could not be comparably to the results we would acquire in the cell, due to less water quantity would have been inside.

So, we decided run the experiment (or calibration) using Hele-Shaw cell, but always manipulating same mixture (therefore, same concentration) and only changing gap between polycarbonate plates, in order to appreciate if we would get hold of the exactly same results, what would come to the conclusion that intensity does not depend on gap width, and then economise time not needing to run some experiments related to all gaps required with all mass fraction dissolution. To corroborate what has been explain, 4 different cell configuration ($0,3$, $0,4$, $0,5$ and $0,75$ mm gap, respectively) were filled with same water-$KMnO_4$ mixture filled. Subsequently, pictures were taken and analysed with *Matlab*. We had 4 images, one for each configuration. It is also remind that when experiments were run, backlighting panel was not available, so a lamp was used. The inconvenient was that the lamp did not provide of uniform lightning to the whole cell, as well as we noticed when pictures were analysed.

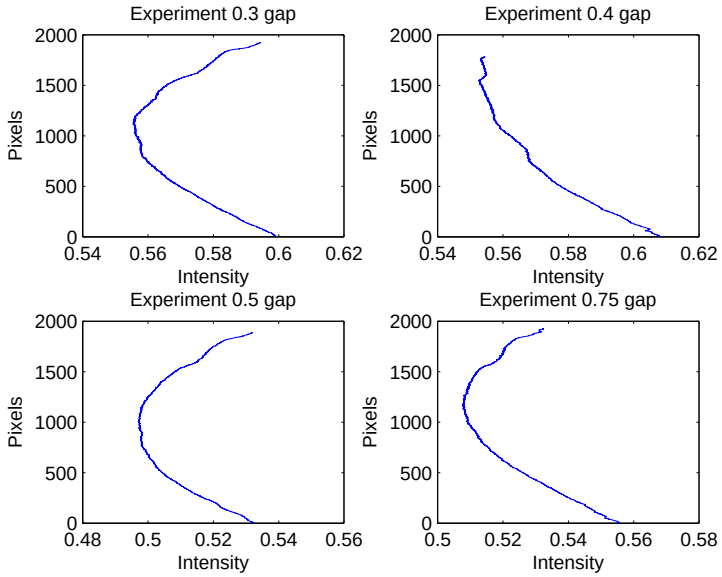

FIGURE 5.2: Comparison of 4 graphics obtained of the images taken in the first mixture calibration. It is represented intensity mean for each matrix row

So, once photos were taken, they were examined. Since we knew that the concentration had to be the same in each pixel, the procedure was the following: for each matrix row, intensity average was calculated and plot the value, getting as values as rows had the matrix. In this way, we could see if there was intensity uniformity through cell height. If light was perfect, the graphic obtained had to be a vertical line. Figure 5.2 shows the results achieved. Although the intensity is different in each case, it was difficult appreciate it in the real images (Figure 5.3). Analysing the plots, we did not have the shape that we expected in any case. However, some conclusion could be extracted of plots. Although a vertical line was not got, experiment $0,3$ and $0,5$ mm gap show a parabolic shape, due to not uniform lightning and the minimum around the middle, but with one strange result: centre of the cell is darker than edges when it is supposed to be opposite (note that in *Matlab* 1 means white and 0 means black). But the rest of the experiments show totally different shapes. In

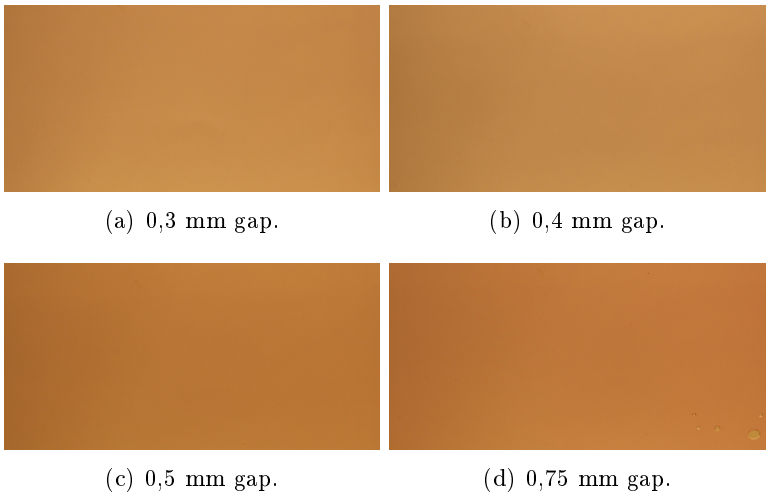

(a) 0,3 mm gap. (b) 0,4 mm gap.

(c) 0,5 mm gap. (d) 0,75 mm gap.

FIGURE 5.3: Images related to Figure 5.2 plots.

0,4 gap experiment, brightness increases through all the height, without explanation, being the behavior totally different to the rest of the graphics. And finally, in 0,75 experiment gap, the shape is not totally parabolic and the minimum is not plotted in the middle, being the bottom part brighter than the upper part. The conclusion extracted was that probably cells were not placed in exactly same position for each experiment, as lamp light. And we also came to the conclusion that the lamp was not good comparing the color and the light of Figure 4.3 and Figure 5.3. Owing to these results, specially 2nd and 4th plots, they weren't taken as a valid results, and after this procedure was repeated, but then with a backlightning panel that provided uniform light.

In spite of the experiments were not valid, intensity cell average was calculated for each experiment, and displayed in Table 5.1. It is possible to appreciate that even though 0,3 and 0,5 experiments had similar curves, they had the biggest intensity cell average, whose error is 10,78 %. And the closest values are from 1st and 2nd experiment although their shapes are the most different. So it is one more point in order to reject the experiment.

TABLE 5.1: Summary of the results after analysed the experiments

gap [b]	0,3 mm	0,4 mm	0,5 mm	0,75mm
Intensity average	0,5704	0,5699	0,5089	0,5218

5.2 Second sampling

It has been explained in Section 5.1, the results obtained in the first sampling to calibrate the mixture were erroneous, so a second sampling was required. To improve the errors made in the experiment before, we had available the backlighting panel. And we wanted to secure all the devices used during the experiment, because although we took care of the devices position, using a ruler and trying that each element would be in the same position for every run, we noticed that sometimes the instruments were placed some millimeters different with respect to the reference position, and then light and pictures could be disturbed. With the laboratory technician help, we fasten the instruments keeping constant the relative position between them. As it is shown in

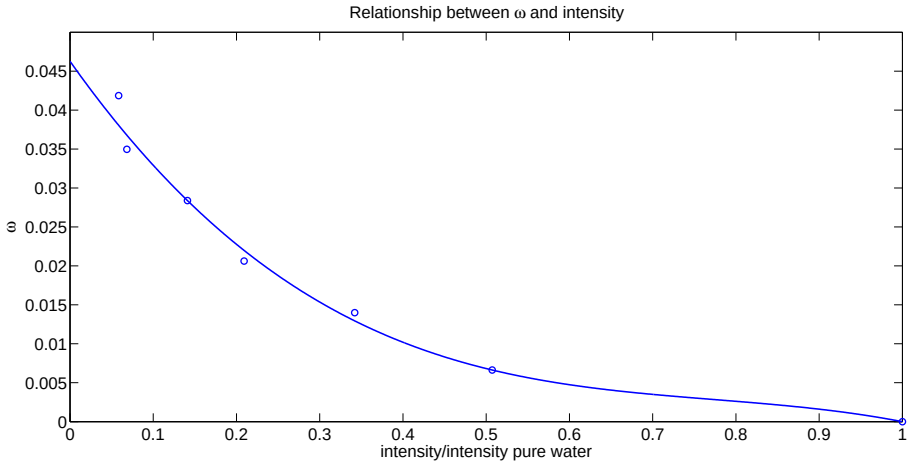

FIGURE 5.4: Relationship between ω and intensities, obtained experimentally, after second sampling.

Figure 6.2, using metallic bars we could secure the support that holds the cell and the camera, and we placed the panel at the end of these bars. We also decided to get ride of tripod, because it was not as stable as the new configuration, since a simple touch could move it and change its position. Then we fasten the camera to the metallic configuration.

So when the configuration was built, we started to prepare the mixtures. The goal, again, was to find, experimentally, the relationship between mass fraction (ω) and the light intensities reached after taking pictures and analyzing them. Then, we could approximate the point found with a function, and afterwards knowing mass fraction for each pixel using that function. Initially, we prepared 10 different mixtures. Obviously, we wanted to increase proportionally the mass fraction from first mixture to last one. To achieve this, we solved Eq. (3.4) to find ω:

$$m_{solute} = \frac{\omega \cdot m_{solvent}}{1-\omega}. \tag{5.1}$$

Then, we weight mass water (equivalent to $m_{solvent}$) using a scale. Once we knew this and ω desirable, and using Eq. (5.1) we calculated the theoretical mass of $KMnO_4$ and after we added the powder until we got the quantity desired. The ω wanted was just an approximation (there is not difference if we plot $\omega = 0,005$ or $\omega = 0,0049$ provided that the mass values were right), and after knew the quantity of powder introduced (column 3 in Table 5.2), we use Eq. (3.4) to calculate the real mass fraction (column 4 in Table 5.2) because then we knew both mass quantities. How it has been explained in Section 3.1, error of measuring the quantities has to be taken into account.Therefore, it is also needed to calculate $\Delta\omega$ (Eq. (3.10)) now that we know the numerically values, and they have been shown in columns 5 and 6. In Table 5.2 are shown all the quantities measured.

TABLE 5.2: Summary of mixture conditions in order to do first calibration.

Exp.	Water [g]	Powder [g]	Mass fraction ($\bar{\omega}$) [-]	$\Delta\omega$ [-]	$\Delta\omega\%$ [-]
1	42,406	0,283	0,00663	$2{,}3{\cdot}10^{-5}$	0,351
2	35,527	0,504	0,01399	$2{,}7{\cdot}10^{-5}$	0,196
3	40,998	0,863	0,02062	$2{,}3{\cdot}10^{-5}$	0,114
4	41,106	1,201	0,02839	$2{,}3{\cdot}10^{-5}$	0,081
5	42,041	1,523	0,03496	$2{,}2{\cdot}10^{-5}$	0,063
6	39,835	1,740	0,04185	$2{,}3{\cdot}10^{-5}$	0,055

Subsequently, we lay the solution for a while in order to obtain a homogeneous and uniform mixed mixture. The problem was that we did not have enough time to run all the experiments, because after each run, we had to disassembly Hele-Shaw cell, clean it because we did not want that anything disturb the results, and assembly it again to be filled of an another mixture and take pictures. To improve the results, 5 pictures were taken for each mixture, to reduce the effect of the light. And we decided to analyze the images taken and see if 6 experiments were enough to find the curve and its corresponding function. Actually, we run 7 experiments, because the first one was with pure water to use it as a reference.

What we did was to calculate the mean intensity value of the whole picture, which it is assumed that is the same, and later calculate the average intensity of the 5 pictures taken for each test. And as we plot X-axis as the ratio between intensity and intensity with pure water, we took pure water intensity average as a reference to use it in the ratio. Next, we wrote in a vector the values of all mass fraction that we had calculated before and with all the points got (7, one for every experiment), we plotted it. The result is shown in Figure 5.4. According to Slim *et al.* (2013), the curve shape found is correct, with being the slope pronounced for lower values of intensity ratios and more stable for higher values. If we use *Matlab* commands, we could find the function that approximates the points thanks to interpolation. In that case, Eq. (5.2) is the result obtained, where x is the ratio between intensities, using a third-degree polynomial function:

$$\omega = -0,0792x^3 + 0,1841x^2 - 0,1512x + 0,0463 \tag{5.2}$$

In this case, the statistical parameters explained in Section1.5.1, to evaluate how good is the approximation, are SSE $= 2,0757e-05$ and adj R-square $= 0,9699$, indicating a good interpolation. However, it is also observed that 7 experiments are not enough to approximate accurately the curve. So it was decided that more tests would be run to obtain a more accurate relationship between ω and the light intensity.

5.3 Third sampling

At the end of the previous section we concluded that more mixtures were needed to better calibrate $KMnO_4$ -water solutions. The procedure was exactly the same that has been explained before, with the only difference that now the mixtures used had a different mass fraction. Table 5.3 sums all the values of the new calibration tests. Comparing both tables, it is visible that in this last test mixtures mass fraction are lower than experiment before and ω is comprised between $\omega = 0,01$ and $\omega = 0,0005$ (theoretically).

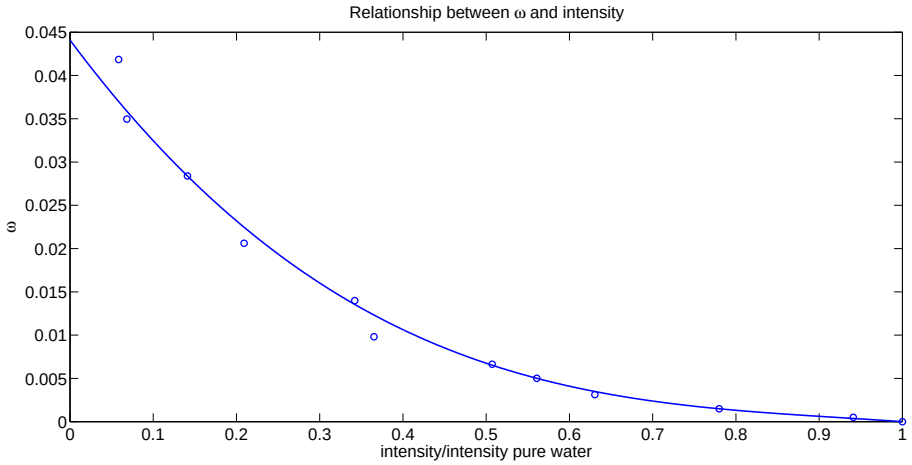

FIGURE 5.5: Relationship between ω and intensities, obtained experimentally, after third sampling.

In Figure 5.5 is shown the new function, where more calibrations points have been used. This points help to get a better shape and better relationship between both parameters. If we see the estimators to evaluating goodness of fit, SSE $= 1.3143e-05$ and adj R-square $= 0,9920$, being closer to theoretical desirable values (0 and 1 respectively). The new function found is reported in Eq. (5.3). But it is also observed that there are 2 points that are a bit far from the curve. One point is the first one starting from the left side. It could be because it is the first measurement, so, by the moment, we do not say that it is wrong. However, the point regarding to $\omega = 0,01$ maybe are wrong, so calibration for this values will be done again.

$$\omega = -0,0476x^3 + 0,1326x^2 - 0,1291x + 0,0441 \tag{5.3}$$

Although even this third sampling was done, we did not still have enough values, so we run more tests, with points mentioned, to get a improved curve.

TABLE 5.3: Summary of mixture conditions in order to do third calibration.

Exp.	**Water** [g]	**Powder** [g]	**Mass fraction** (ω) [-]	$\Delta\omega$ [-]	$\Delta\omega$% [-]
7	44,719	0,443	0,00981	$2{,}2{\cdot}10^{-5}$	0,224
8	36,945	0,186	0,00501	$2{,}7{\cdot}10^{-5}$	0,535
9	39,259	0,123	0,00312	$2{,}5{\cdot}10^{-5}$	0,810
10	41,508	0,062	0,00149	$2{,}4{\cdot}10^{-5}$	1,61
11	37,898	0,019	0,00050	$2{,}6{\cdot}10^{-5}$	5,261

5.4 Fourth sampling

In this new calibration tests, 3 tests were done, with corresponding values shown in Table 5.4. The main goal was to correct the point regarding to $\omega = 0,01$ just in case the measurement done before was wrong, add an extra point between $\omega = 0,015$ and $\omega = 0,02$ and see if point with the highest value of mass fraction was right. For the moment, more points with $\omega > 0,045$ were not added because, according to Slim *et al.*

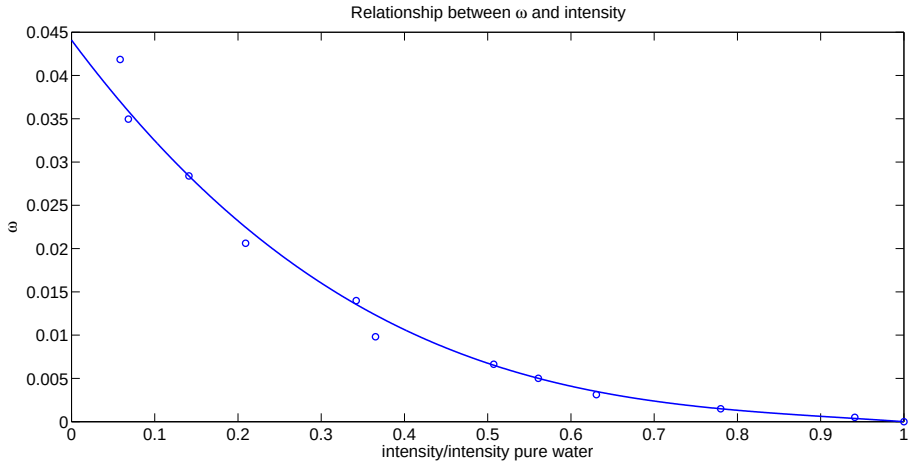

FIGURE 5.6: Relationship between ω and intensities, obtained experimentally, after fourth sampling.

(2013), sensitivity for small values of ratio intensities is really low, and a minimum error in this ratio cause a big error in ω. However, do not get results for this zone also cause an error, because reading the function maximum mass fraction is around $0,45$, and we know that is wrong. After analyse both error, we thought that is better do not calibrate the mixture for smaller values of ω, due to the error is smaller in that case.

TABLE 5.4: Summary of mixture conditions in order to do third calibration.

Exp.	**Water** [g]	**Powder** [g]	**Mass fraction** (ω) [-]	$\Delta\omega$ [-]	$\Delta\omega\%$ [-]
7	41,779	0,436	0,01033	$2{,}3{\cdot}10^{-5}$	0,227
8	39,013	0,674	0,01698	$2{,}5{\cdot}10^{-5}$	0,146
9	37,231	1.770	0,04538	$2{,}5{\cdot}10^{-5}$	0,054

Eq (5.4) is the last formula found to relate ω and intensity, almost equal to eqwint2, also visible in Figure 5.6

$$\omega = -0,0474x^3 + 0,1322x^2 - 0,1289x + 0,0441 \tag{5.4}$$

5.5 Light intensity correction

Although the images had pretty constant values, referred to their intensity, for intermediate values of color (not even so bright not even so dark), some colour (intensity) gradients could be appreciated in the image. Applying the command *contour* to the original image, it is observed the difference of colours, which it means that it is not totally homogeneous and the shape of distribution of the intensities, illustrated in the first image of Figure 5.7. Then, using the command *cftool*, the aim was to find an equation to approximate the image contours. This equation, depending on the variables x and z (length and height cell, respectively), has the configuration of Eq. (5.5). How it is shown, it is a 3rd polynomial equation, where p_{ij} are the different coefficients. This procedure was done for each mass fraction pictures used to calibration,

using always the same from of the equation. We believed that this equation was good because the worst "GOF" (goodness of fit), parameters to evaluate the accuracy of an approximation, were Adjusted R-square = 0,9385 and RMSE = 0,007165. Moreover, Figure 5.7 shows the comparison between the original and the interpolation contours, being almost the same.

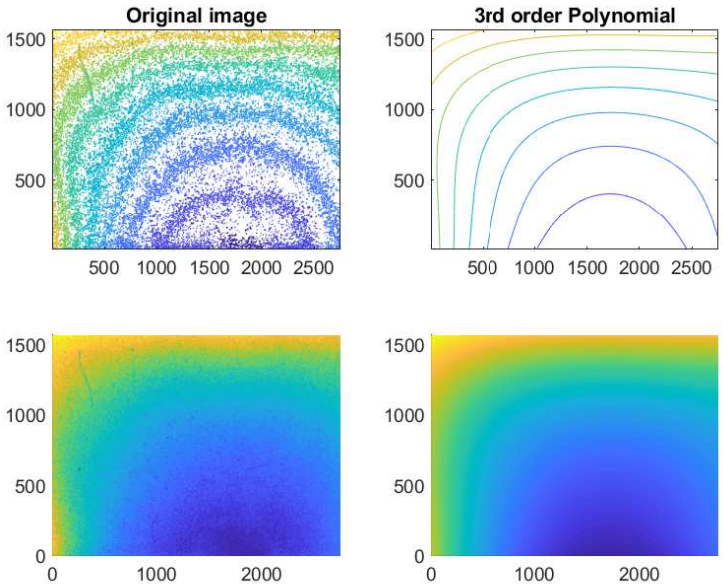

FIGURE 5.7: Comparison of the contour applied to the original picture (left) and the equation found, which reported in Eq. (5.5). In this case, $\omega = 0,02839$.

$$f(x,z) = \mathrm{p}_{00} + \mathrm{p}_{10}\cdot x + \mathrm{p}_{01}\cdot z + \mathrm{p}_{20}\cdot x^2 + \mathrm{p}_{11}\cdot x\cdot z + \mathrm{p}_{02}\cdot z^2 + \\ + \mathrm{p}_{30}\cdot x^3 + \mathrm{p}_{21}\cdot x^2\cdot z + \mathrm{p}_{12}\cdot x\cdot z^2 + \mathrm{p}_{03}\cdot z^3 \qquad (5.5)$$

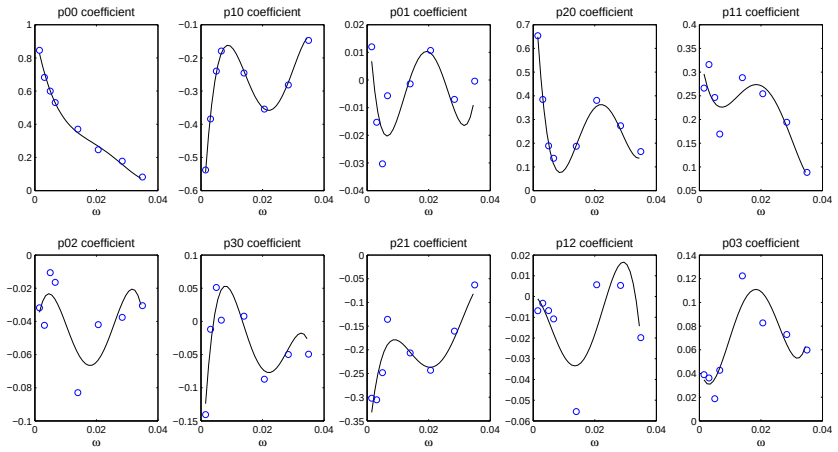

FIGURE 5.8: Relationship between coefficient values and ω for each coefficient.

Then, once found all the parameters for all images, what we wanted to observe was if there was a good relationship between mass fraction and each parameter. If there was, knowing the mass fraction, we could know the value of the coefficients (p_{00}, p_{10}, etc.) and with the aid of Eq. (5.5) we could find the real intensity value. However, as shown in Figure 5.8, only coefficients p_{00}, p_{10} and p_{20} are well approximated, in contrast with some another coefficients such as p_{01}, p_{11} or p_{02} are really bad approximated. And even so, we expected a relationship with a curvature similar to p_{00} coefficient, monotonic, and not as p_{10} or p_{20}.

The results presented in Figure 5.8 clearly show that the form adopted to approximate the function is not a good candidate. However, p_{00} has precisely the form of Eq. (5.4). Therefore, we can consider the present method as a general method that, although has still to be improved, may describe faith fully the light intensity within the cell.

Chapter 6

Experimental set up

The experiment will be run in a Hele-Shaw cell. In consists in two polycarbonate plates, whose size could be chosen as convenience. The polycarbonate glass was chosen as the plate material because its resistance to the $KMnO_4$-water mixture and its transparency. The distance between two plates, how it as mentioned, will be indicated as b, and it will be changed in order to modify Ra and reach different Rayleigh numbers. The thickness has to be kept accurately constant through all the cell. Besides cell has to prevent any kind of leakage. On the top of the cell a grid will be hold between the two plates and $KMnO_4$ powder will be put on it, and later mixture will form when water contact it. Water will be brought in the cell with a syringe from a lower corner.

6.1 Experimental Hele-Shaw cell

Although it was clearly known how Hele-Shaw cell was, there were different possibilities to get it. It was also known that use silicone could be the best option in order to avoid any leakage of liquid, but using it implied a more complicated plate structure, because a kind of hole was needed to introduce the silicone. We have to imagine that the initial plate was totally flat and all the holes needed had to be made by a laboratory technician with machines like milling machine. And after each experiment silicon had to be removed, because we had to change the shim to modify b. So, silicone had to be warm again and afterwards, clean the glass. Because of all this things, first cell was made without silicone, and the aim was to observe how fluid developed and if any leakage was produced. Then, this first cell was composed of: two polycarbonate plates, whose size was 90x190x30 mm, 3 stainless steel shims, whose aim was close the cell on the bottom and two sizes and modify b gap depending on its thick and 5 screws in order to tighten both plates . 2 shims were placed vertically in each side and the other one was placed horizontally on the bottom. And about screws, a laboratory technician made 5 holes in the glasses, one on each corner and last one in the middle base position. Obviously, 5 holes were in the same position in both plates. With this techniques, the real cell sizes were 60 x 175 mm. Figure 6.1 shows the final structure of the cell. In section 'First experiment' is explained in detail the problems that this configuration presented.

Otherwise, the devices used to take pictures were the cell, a backlightning panel, a cell support to hold it, the camera with its corresponding support and some rails where to affix everything, thank to some screws. Figure 6.2 shows the place of each device and the relatives lengths between them.

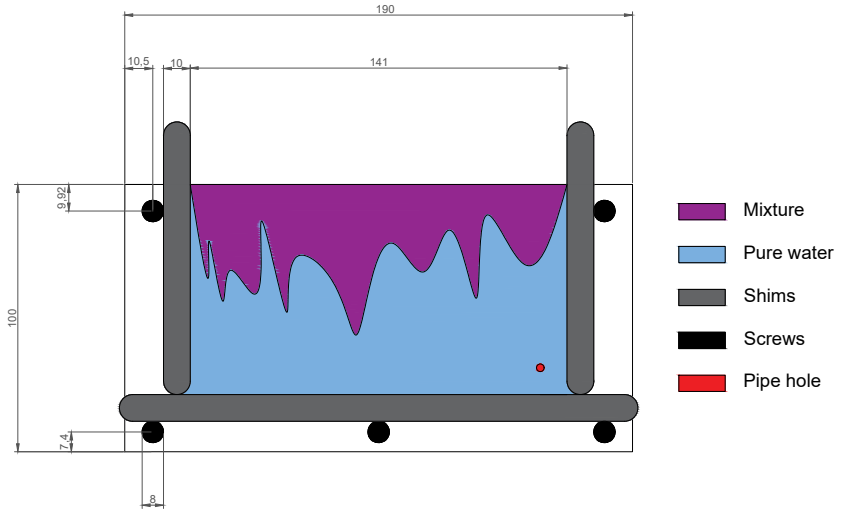

FIGURE 6.1: First Hele-Shaw cell configuration while first experiment were being run.

6.2 Camera

A camera is needed to take pictures or to record the development of the mixture in time. In our case, the camera used is a Canon EOS 1300D. About the sensor, the camera has a resolution of 17,9 megapixels, which means 5184 x 3456 effective pixels. On the other hand, it has a video resolution of 1920 x 1080 pixels (25/30fps). ISO setting could vary from 100 to 6400. Images were taken with a camera shutter, whose shutter speed was 1 image per second in our case. The camera was mounted on a kind of affix tripod (Figure 6.2) facing the centre of the cell to facilitate the mixture progress recording.

6.3 Solute powder

The powder used in order to run the experiments and to simulate the CO_2 underground conditions is potassium permanganate. Every time that we run any experiment using this material, it has to be ground, because some times there are big stones due to the grains are joined.

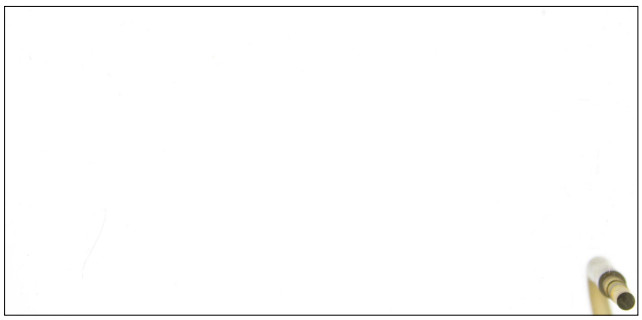

FIGURE 6.3: Cell image when it is empty of water, showing that the backlightning panel provides well white light.

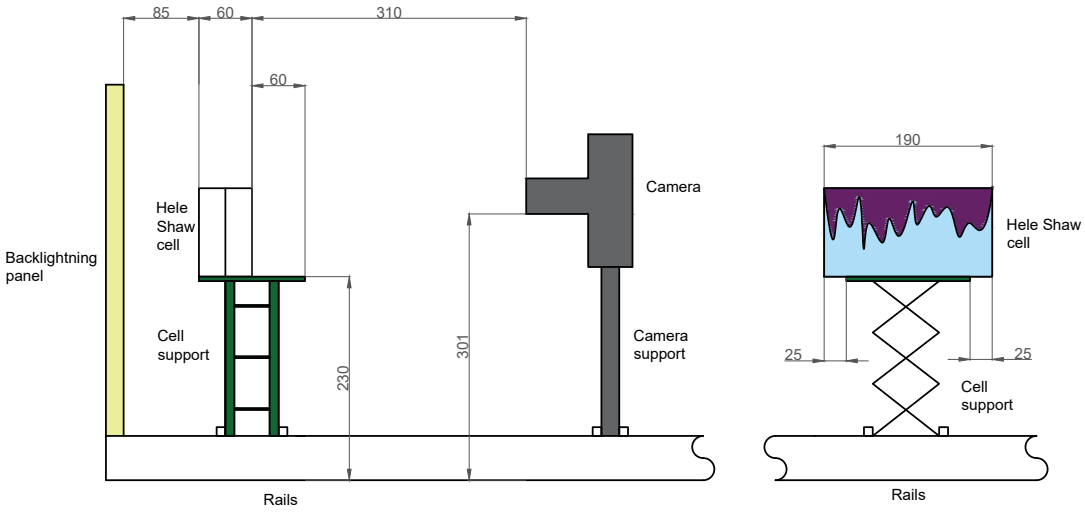

FIGURE 6.2: Configuration of the devices used during experimental and calibration tests

6.4 Backlighting panel

In order to obtain an almost perfect light intensity in the cell to improve the pictures quality done by the camera, a backlightning panel is used. The panel, shown in Figure 6.2, is 440 x 350 mm, big enough to cover and illuminate the whole cell surface. As shown in Figure 6.3, it provides a perfect white image when the cell is full of water or when it is empty.

6.5 Cell cleaning

At the end of each experiment, the cell was emptied and the rig was disassembled. Later plates, screws and shims had to be cleaned. Soap, water and paper were used too. Glass was the most important equipment that had to be accurately cleaned, in order to do not disturb next experiments. After cleaning, they were left drying. During the cleaning process, plastic gloves should be used due to effect of $KMnO_4$-water mixture with skin, that it was not poisonous but skin changes its colour to brown color for a few days.

Chapter 7

Analysis of experiments

In this section we will explain all the experiments that have been run, interpreting the experiments as the process of simulating the real dissolution of CO_2 in brine. When the Hele-Shaw cell is filled with water, which interacts with $KMnO_4$, fingers appear, and we study the behaviour of the mixture from onset until the whole saturation. Then, in this chapter we do not perform experiments as the process of filling the cell with the mixture done, as we did in order to calibrate the mixture, light calibration, etc. but the whole process of finger formation, with different modifications between them. We wanted to get four characteristics mainly: the first one, that powder did not fall down inside the gap before the mixture onset. The second one was getting constant rise of water along all the cell in order to obtain the contact between water and $KMnO_4$ at the same time along all gap surface. Third one, that fingers development was vertical instead of inclined. And finally, that powder was well distributed along the gap, with approximately same amount in every point.

7.1 First experiment

Cell configuration is shown in Figure 6.1. It was also used a camera, a lamp and a white background. Inside the problems that we had building it, we had to ensure a really good contact between shims to avoid leakages, and screws had to tighten enough both plates. But, leakage would happen for sure. When we were running the experiment, we noticed that mesh pore size was too big because when we put the mineral in it, some powder fell down into the cell and some mixture appeared before the beginning of the experiment, so it was changed to another mesh with small pore size. And another difficult task was camera configuration, because focus had to be done accurately to get pictures as much clear as possible. And when test had been run, two big problems appeared: in spite of efforts to tighten screws, small leakages happened through contact between vertical and horizontal shims, in both sides. And a second problem was that the hole made to put the syringe in and inject water was so far from the corner, so the region around it was really disturbed by its influence, and mixture in this zone could not be kept in mind to analyse the results, so we decided that in the final cell, hole had to be closer to the corner to decrease its influence.

Afterwards, in spite of troubles got, the pictures were analysed with *Matlab*. With the software, once pictures were cropped to focus just the cell, concentration was calculated. *Matlab* reads an image as a matrix and colour figure has 3 matrix (for red, green and blue color, respectively, because it uses rgb system) whereas black and white portrait only has one matrix. So, first of all, it was necessary to convert rgb picture into gray picture because it was not possible associate intensity (or concentration) if 3 matrix were taken into account. Subsequently, intensity was calculated according to matrix values. These values were compress between 0 and 1, and as *Matlab* works, 0

means black and 1 means white. So, if we want to associated intensity to concentration, best and easiest option is multiply intensity by maximum concentration, which means that black is maximum concentration and white zero concentration. To proceed in this easy way, 1 has to be black. So this technique was applied to each matrix value: $p_c = |p_o - 1|$, where p_c is the new value in the scale wanted and p_o is the old value, that is, value calculated by *Matlab* at the beginning. After this, we had the matrix in the desired format. When a picture is taken, although we used a white background, in the part where we only have water inside, the color was not totally white, so *Matlab* read it as a color, assigning a value to this picture, and although this value was closed to 0 (in new format), it was not 0, this means that there was some concentration when, in fact, there was not. So a filter had to be applied and its function was to convert the pixels with lower values to 0, meaning, convert pixels where there were not any $KMnO_4$ substance yet into pure white (without concentration there).

As previously explain (Figure 2.1), this first procedure was changed in order to find an accurate way to calculate the total amount of $KMnO_4$ inside the cell, such as the concentration and flux.

7.2 Second experiment

The second experiment was focus on the initial condition, i.e. on the onset of the dissolution phenomena. The problem that we found was that when we put the powder on the grid, mesh holes were not small enough and some grains fell down through the cell, disturbing the results even before the real interaction took place. We tried to fix this problem using a second grid, one above each other, and moreover holes were smaller. First we place both grids together, subsequently add the powder as much distributed as possible, and later put the ensemble on the grid. It could be a good option, because the powder grains smaller than pore size fell down before. The problem was that the transport of the ensemble had to be really accurate because, since grains weight was so small, a minimum contact to the grid causes that powder jump, falling down.

So, further alternatives were considered. The first one was to put first the grid on the upper part of the Hele-Shaw cell, and affix it with sticky tape. After, we put the powder on it, but not just above the gap but in one extreme. Finally, we added slowly the water, and when it reaches the surface, we pushed quickly the powder with a tool, trying that along the whole gap surface interaction took place. However, in spite of this procedure, the contact was not uniform along the entire space, starting the finger formation in one side, and as soon as we put the powder, since the grid was not totally rigid, despite the sticky tape, the first fingers were formed a bit horizontal instead of totally vertical, as it is shown in Figure 7.1.

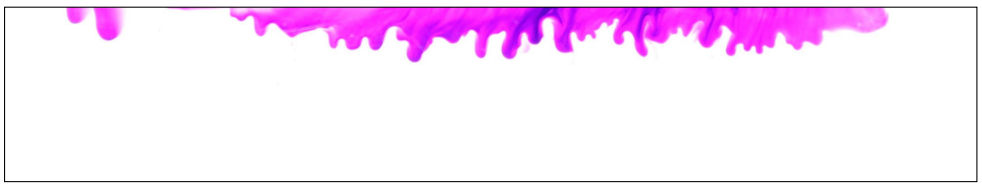

FIGURE 7.1: Fingers head are a bit inclined instead of be totally vertical.

Then, a different option that was considered was to put first powder on the grid and throw few drops just to wet the $KMnO_4$. Then, in the cell, add water until it overflows a bit on the top. Subsequently, move the grid and place it carefully on top of the cell, and let that pure water and wet powder interact forming fingers. The main aim of this was avoid that grains fall down at the beginning. However, it did not work as it could be seen in Figure 7.2 where all that small fingers in (a) mean that powder fell down before real interaction started, disturbing results. In (a) image, only fingers made at the right can be assumed as well. In contrast, image (b) shows how image should have been since beginning, although some thin fingers are still. Both images are separated by a 8s interval.

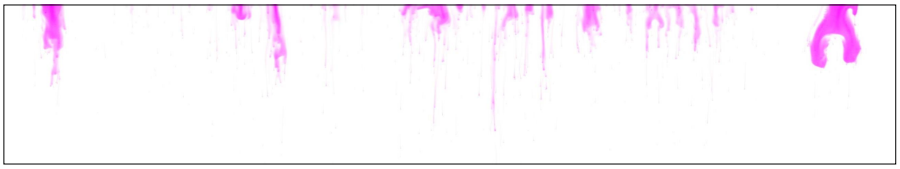

(a) Thin fingers formed by grains

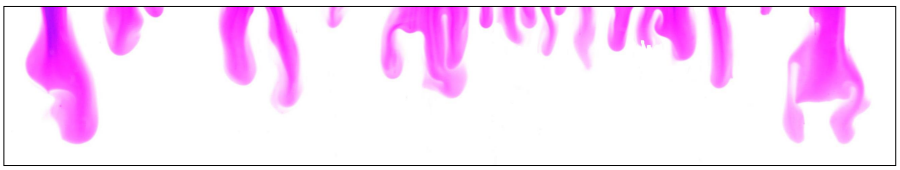

(b) Fingers formed as we expected.

FIGURE 7.2: Development of the mixture with 8s of difference between two images when wet powder was used.

How this both methods did not resolve the main circumstances that we had to guarantee, further options were tried. To solve the problematic of same quantity of powder, the following option was tried: a rectangle, whose size was 5 mm x gap width approximately, was cut in a paper. Then, the paper was put in the cell, but not just on the gap but in one side, and we distributed powder in that hole. Later, we overflowed water from the gap and then we pushed powder with a rigid bar to the water, but the substances did not mix uniformly. Figure 7.3 shows the configuration explained, where color black represents both plates, grey represents surface gap occupied by shims, color blue represent paper stencil and purple the gap where powder is placed. Overflowed water has not been drawn to simply the sketch.

A different option that we attempted was create a kind of handmade "hole" above one plate using two walls. The goal was put as the powder as we wanted without concern about grains fell down through the gap and water interacted with it because was separated by a wall. Two walls were used, one to separate both substances and second one to avoid that water spilled through the plates face. After it, we overflowed water until in one wall side we had water and powder in the another one. Finally, we left the wall and inject a bit more water in order make a uniform contact line and after mixture happened, release some water with a syringe to let the mixture flow through the gap. Using this technique, we avoid grains size effects, but we did not get that mixture flows uniformly since the beginning along all gap surface, starting fingers just in the middle. A configuration sketch is shown in Figure 7.4, where black colour represents, again, the two polycarbonate plates, red is associated to both walls

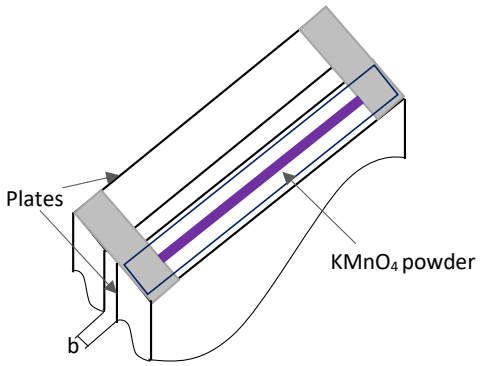

FIGURE 7.3: Sketch of the configuration when we used a paper as a stencil.

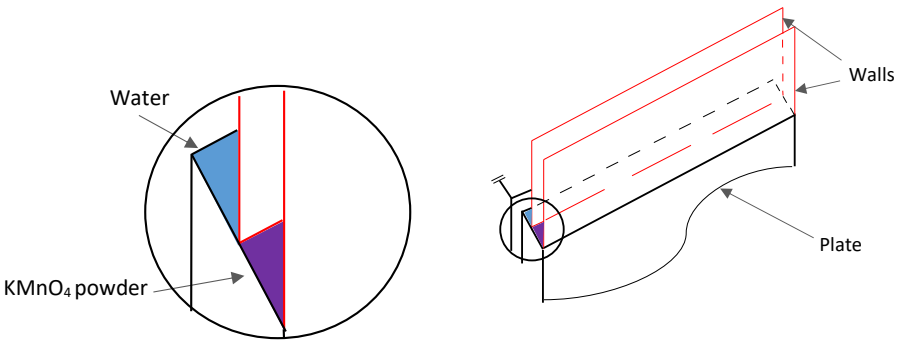

FIGURE 7.4: Sketch of the configuration using walls to separate water and powder

to separate substances, blue is the part where water overflowed and purple is the place where powder is collocated.

Finally, leveraging configuration drawn in Figure 7.4, an alternative was thought. The point was, instead putting powder in the middle hole, add there a over-saturated $KMnO_4$-water solution, before prepared in a vase and ensuring that it was over-saturated, and once we moved away the wall, let that both liquid substances get in contact with each other. We expected that since the amount of mixture was well distributed in the hole, when we moved away the wall they would flux uniformly, and falling down also uniformly through the gap. And it was what happened. Then, we had to avoid grains and constant flow issues. However, the problem that we found was that after a long time while process was happening and forming fingers, the concentration inside the cell was so light. We expect that after enough time, dissolution inside the cell has to be almost saturated, but in this experiment the mixture was approximately half saturated (without analyze results, just with view). And we did not know if it happened because few amount of mixture was placed there or because always happened like that. Anyway, test was also rejected, with need of find a solution.

Due to constant increase water flow problem, in all the experiments that were run

that day, first of all we caused that water overflows of the cell, distribute it along the gap surface and finally add the powder, using different techniques.

The first idea that it was thought was add the powder as a compact block. To get this, we decided to wet the powder. But how we just wanted to wet the powder instead of create the mixture, small amount of water should be used. Then, what we used was a spray gun with water as a liquid. After, we used a hard paper which function was that the compact block stick in it, being a kind of wall, and a metal to press the wet powder against the hard paper. Figure 7.5 illustrate simply the configuration, were white colour is the hard paper, grey is the metal and purple is used to $KMnO_4$ powder. The arrow represents the movement of the metallic part. Later, when powder was stuck, we moved the ensemble and placed it carefully on the top of the cell and wait for the dissolution. However, we had two problems. The first one was that the amount of powder was small, and we got a really low-concentration solution. Moreover, due to hard paper material, it sucked mixture to itself instead of let that dissolution flowed inside the gap. The last disadvantage was that the movement of the hard paper had to be so quickly because how the compact powder was quite wet, and if we waited some many time, the block unpicked, falling grains or amount of powder when we did not want it.

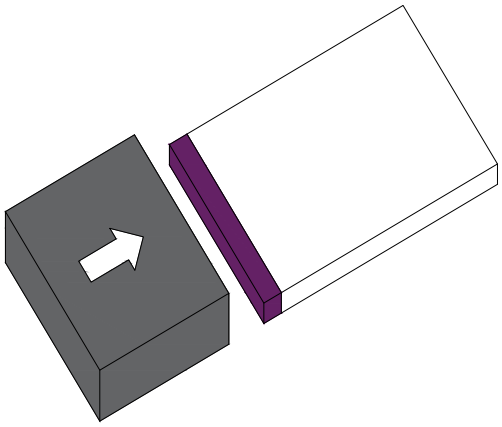

FIGURE 7.5: Sketch of the configuration to compact the powder in the hard paper

Next option was tried consisted in to use a straw and the grid. The idea was to roll the grid inside the straw and to do a thin cut along the straw. Later, fill it with powder until all space inside was covered. Once all this process was done, we added water inside the cell until it overflowed, distributing the water through all the upper flat space and placing the wrap there, not exactly in the gap. Its position had to ensure that the cut was in the bottom part in order to let the contact between water and $KMnO_4$. In this way, we ensured that powder was well distributed. The problem that appeared was that there was not enough contact between both substances and then the mixture was little saturated. Moreover, due to the wrap material, it sucked out the mixture to itself instead of let it flows down through the gap. In Figure 7.6 is shown the configuration, where green object represents the wrap and it is possible to see that the grid (grey color) is a bit longer than the wrap. The powder is supposed to be inside and it is not possible to see the cut.

Finally a better option was found. It consisted in making a small triangle in the glasses (Figure 7.7, in the inner part, where water flows up through. Then, the grid, which it is not totally rigid, is placed in this triangle, taking advantage of this shape,

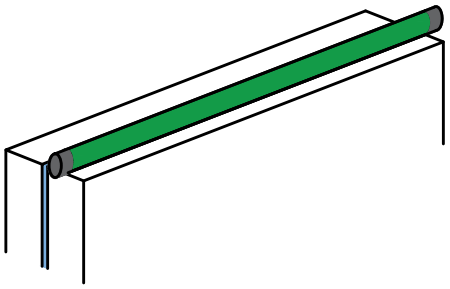

FIGURE 7.6: Sketch of the configuration using the wrap and the grid rolled.

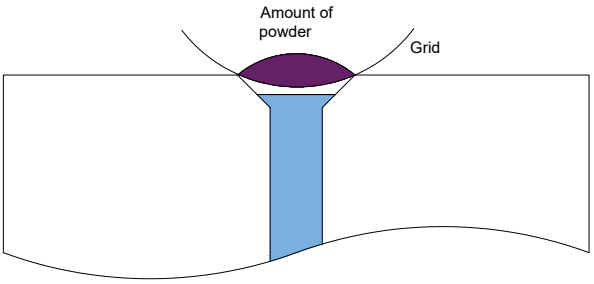

FIGURE 7.7: Side view of the upper cell configuration, where the triangle shape in both plates is visible.

and then, once it is placed, it has not moved itself. Moreover, using so much quantity of powder we ensure that there will be powder well distributed, without working out well that central part has more amount of. Then, we put $KMnO_4$ on the grid and we moved the assembly configuration. But before laying it, we put a paper on the gap in order to avoid that small stones of powder fall down the gap due to its size is smaller than pore grid size. Then, we move away the paper and we place the ensemble. In the previous configurations, first we added the water and later we placed the grid. But how we do it manually, due to the pulse it is really difficult put the grid totally flat, without any part touches the water before, since then fingers in that part will appear first and results will not be good, so first we lay the grid and afterwards we add water. If we had more complex devices which allow to take it down slowly and flat, water could be added first. Furthermore, water should be added slowly.

7.3 Results

We expected to run experiments with the same cell structure, but higher than the cell used during simulations and calibrations (Figure 6.1) and changing b in order to change Ra number and then compare the results with a dimensionless parameter. We also wanted to run the experiment with the good grid configuration found. Because of the time we could not run and analyse the experiments as we expected. In spite of this, one of the simulating test was anaylse. The characteristics of the experiment

were that the height cell (H) was 70,6 mm, $b = 0,4$ mm and it was done during 261 s. Because of this time, we did not achieve the fully saturated mixture inside the cell. The development of the mixture in time is shown. The original images (Figure 7.8), the concentration along the Z-axis (Figure 7.11) and the amount of mass (Figure 7.9) are reported.

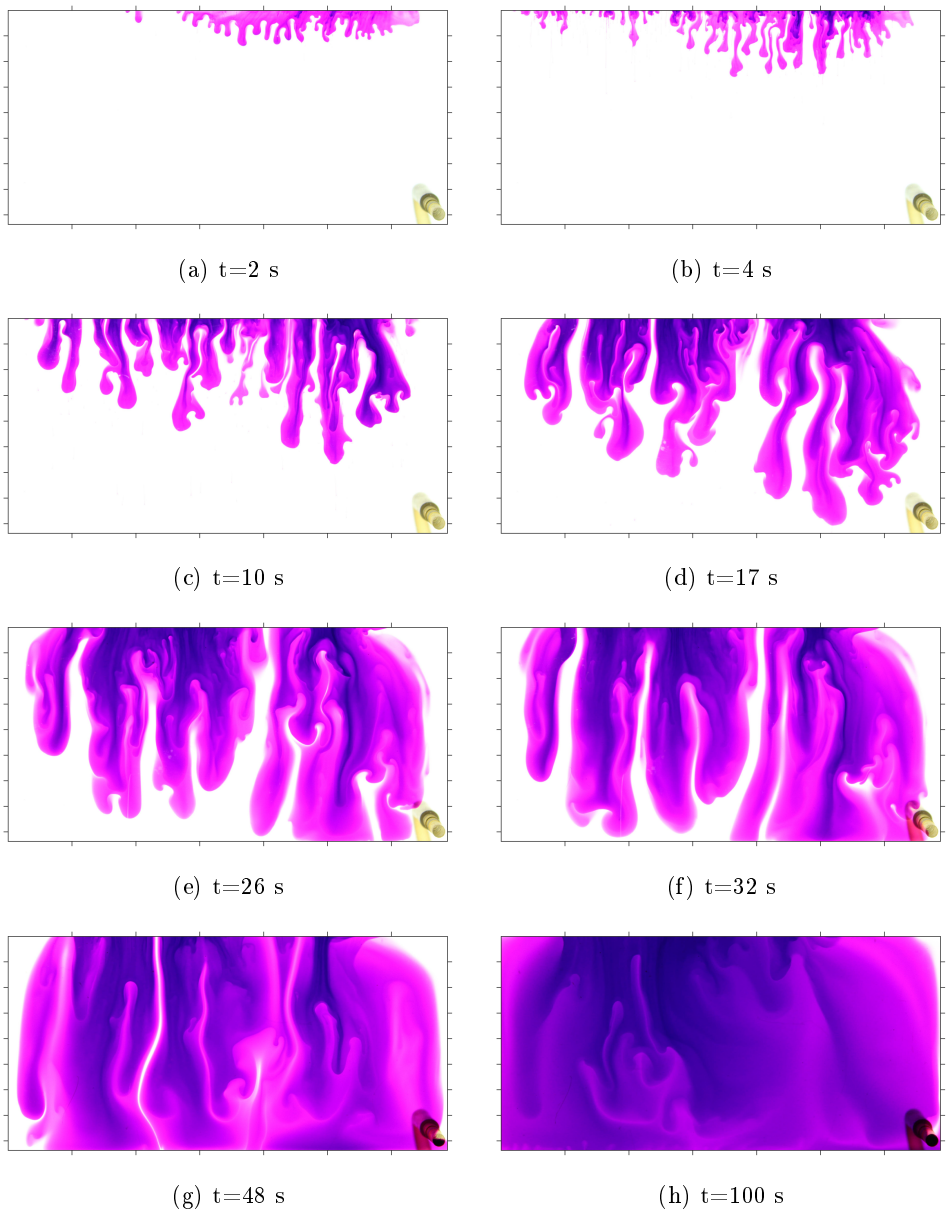

(a) t=2 s (b) t=4 s

(c) t=10 s (d) t=17 s

(e) t=26 s (f) t=32 s

(g) t=48 s (h) t=100 s

FIGURE 7.8: Evolution of the system time. The concentration field C(x,z) is shown in corresponds of different time instants, from onset (t=2) to shutdown (t=100 s).

In Figure 7.9 is visible the evolution of the mass in time, noticed by the points that follow the 3 curves. This 3 curves, widen in the Figure 7.10, distinguish three different regimes according to De Paoli *et al.* (2017). The first one is diffusive regime, at the beginning, where the flux is decreasing if we compare the difference density between the top (where concentration is equal to 1) and the the point that is below it (where concentration is equal to 1). After that, we appreciate the constant regime, where the density difference between these two points slightly changes. And finally

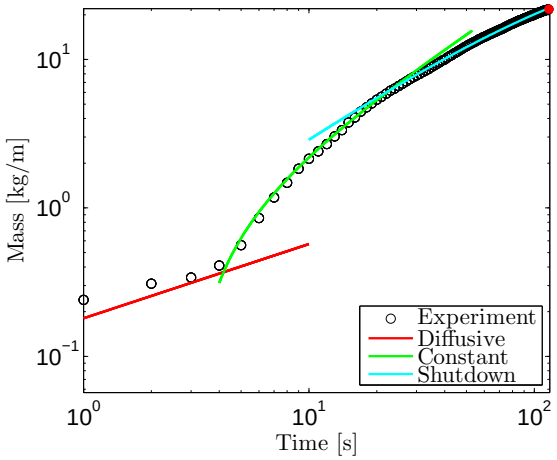

FIGURE 7.9: Evolution of the mass of $KMnO_4$ dissolved in water in time.

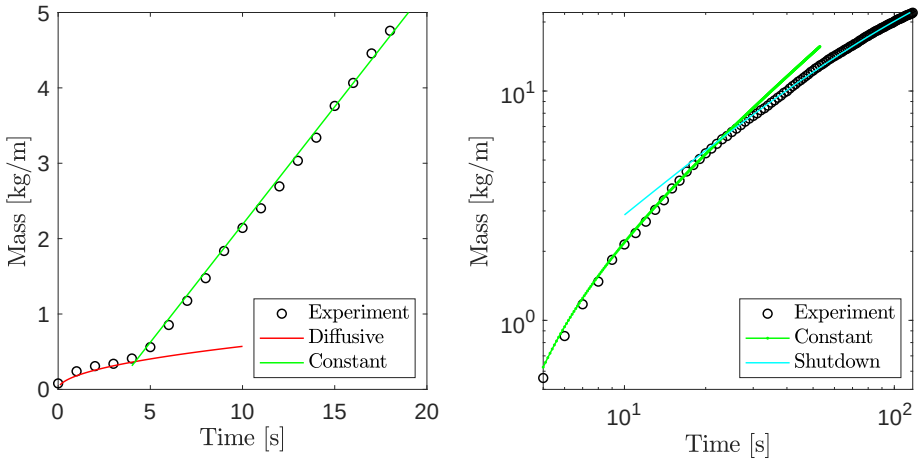

FIGURE 7.10: A close up view of the dissolution process is proposed in order to appreciate the 3 regimes: diffusive regime, constant regime and shutdown.

the shutdown regime, where the flux is decreasing. And it is useful to note that in Figure 7.9 and in the right image of Figure 7.10, the axis are in logarithm scale, and that is why, for example, the green line (constant) is not a straight line.

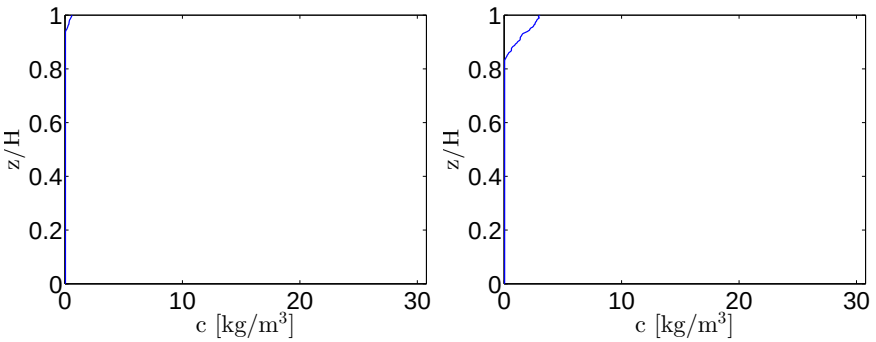

(a) t=2 s

(b) t=4 s

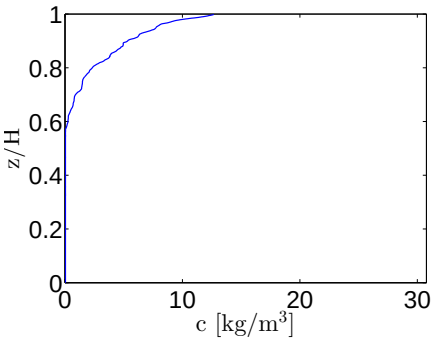

(c) t=10 s

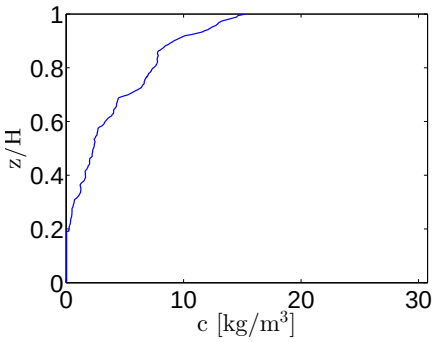

(d) t=17 s

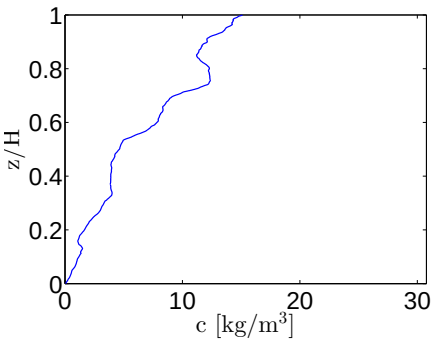

(e) t=26 s

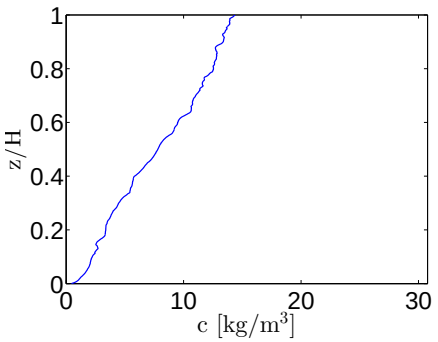

(f) t=32 s

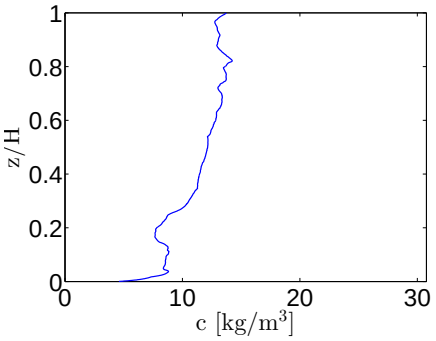

(g) t=48 s

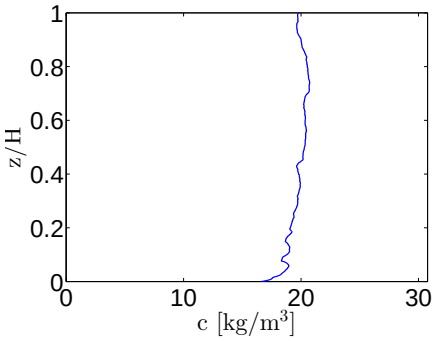

(h) t=100 s

FIGURE 7.11: Evolution of the horizontal-averaged concentration profile as a function of the wall normal coordinate. Profiles are shown for different instants of t.

Chapter 8

Conclusions

We can sum up the thesis we have achieve a good structure of the cell to avoid leakages and to facilitate the $KMnO_4$-water mixture, abiding by the circumstances that have been explained in Section 7.2. We also have noticed the influence of the backlightning panel on the results achieve, because the results got using the lamp were so bad and we could improved them using the panel. However, it does not provide a totally uniform light intensity, so it is important work on it because although the intensity gradient in the pictures is so small, it disturbs a little bit the results. About calibration, the relationship between the intensity and ω was exactly as we expected. Maybe for really low intensity values ($<$0,01) it could be better approximated, but the error made in this short regime is small due to the high sensitivity between mass fraction and intensity and the fact that the main quantity of values are out of this range. Only we could find points in this regime at the end of the experiment, when the mixture is almost fully saturated. Finally, we have found 3 regimes (diffusive, constant and shutdown) in the experiments, same regimes that were found by Slim (2014) and De Paoli *et al.* (2017) in their numerical work.

8.1 Future researches

Although important progresses have been done during the work, they are not enough in order to compare the experimental results with the numerical results found using *Matlab* by the institute department before starting on working on this thesis. The main progresses have been the calibration done in the mixture calibration (Chapter 5), but specially in the way to start the mixture and to write the *Matlab* code. This first one has caused a lot of problems that we did not expect at the beginning. It was so difficult to find a good option to place the grid with $KMnO_4$ powder without grains fell down, such as how achieve the fact that water rises up uniformly to the upper part. Finally, with the configuration described in Figure 7.7, we got a good structure. However, an improvement could be applied: instead of placing the grid manually design a simply structure that allow to go down the grid slowly and uniform, hold the tow sides.

On the other hand, some parts should be improved. The main process that should be improved is to correct the light intensity described in Section 5.5. The results presented in Figure 5.8 are not satisfactory. However, the first image in this figure has precisely the form that we expected. So it is possible to consider the method followed as a general method, but it is obvious that some changes should be done on it, like to use a different equation than 3^{rd} polynomial function.

And the other work that I encourage to do is to make the real experiments, with the appropriate specifications. This specifications are to use a higher cell and run different experiments changing the gap (b) to obtain distinct values of Rayleigh number (Ra) and compare then the results. To facilitate this task, I encourage to take advantage

of the work done and described in this thesis, how for example the code, the mixture calibration or the procedure that should be followed to obtain a good dissolution onset.

Bibliography

Andres, Jeanne Therese H, & Cardoso, Silvana SS. 2011. Onset of convection in a porous medium in the presence of chemical reaction. *Physical Review E*, **83**(4), 046312.

CCP. 2015. *Large-scale CCS facilities*. urlhttps://www.co2captureproject.org/co2_trapping.html .

Chan Kim, Min, & Kyun Choi, Chang. 2012. Linear stability analysis on the onset of buoyancy-driven convection in liquid-saturated porous medium. *Physics of Fluids*, **24**(4), 044102.

Cheng, Philip, Bestehorn, Michael, & Firoozabadi, Abbas. 2012. Effect of permeability anisotropy on buoyancy-driven flow for CO2 sequestration in saline aquifers. *Water Resources Research*, **48**(9).

Cherezov, Ilia. 2017. *Modelling Convective Dissolution and Reaction of Carbon Dioxide in Saline Aquifers*. Ph.D. thesis, University of Cambridge.

Ching, Jia-Hau, Chen, Peilong, & Tsai, Peichun Amy. 2017. Convective mixing in homogeneous porous media flow. *Physical Review Fluids*, **2**(1), 014102.

CIA, Central Intelligence Agency. 2015. *The World Factbook*. urlhttps://www.cia.gov/library/publications/the-world-factbook/.

De Paoli, Marco, Zonta, Francesco, & Soldati, Alfredo. 2016. Influence of anisotropic permeability on convection in porous media: Implications for geological CO2 sequestration. *Physics of Fluids*, **28**(5), 056601.

De Paoli, Marco, Zonta, Francesco, & Soldati, Alfredo. 2017. Dissolution in anisotropic porous media: Modelling convection regimes from onset to shutdown. *Physics of Fluids*, **29**(2), 026601.

DOE. 2018. *Pre-combustion CO_2 capture*. urlhttps://www.netl.doe.gov/research/coal/carbon-capture/pre-combustion.

Duan, Zhenhao, & Sun, Rui. 2003. An improved model calculating CO2 solubility in pure water and aqueous NaCl solutions from 273 to 533 K and from 0 to 2000 bar. *Chemical geology*, **193**(3-4), 257–271.

Elenius, Maria Teres, & Johannsen, Klaus. 2012. On the time scales of nonlinear instability in miscible displacement porous media flow. *Computational Geosciences*, **16**(4), 901–911.

Ennis-King, Jonathan, Preston, Ian, & Paterson, Lincoln. 2005a. Onset of convection in anisotropic porous media subject to a rapid change in boundary conditions. *Physics of Fluids*, **17**(8), 084107.

Ennis-King, Jonathan P, Paterson, Lincoln, *et al.* 2005b. Role of convective mixing in the long-term storage of carbon dioxide in deep saline formations. *Spe Journal*, **10**(03), 349–356.

Farajzadeh, Rouhollah, Salimi, Hamidreza, Zitha, Pacelli LJ, & Bruining, Hans. 2007. Numerical simulation of density-driven natural convection in porous media with application for CO2 injection projects. *International Journal of Heat and Mass Transfer*, **50**(25-26), 5054–5064.

Gapminder. 2018. *Gapminder*. urlhttps://www.gapminder.org/tools/.

Garcia, J. E. 2003. Fluid dynamics of carbon dioxide disposal into saline aquifers.

Ghesmat, Karim, Hassanzadeh, Hassan, & Abedi, Jalal. 2011. The effect of anisotropic dispersion on the convective mixing in long-term CO2 storage in saline aquifers. *AIChE journal*, **57**(3), 561–570.

Gorrini, Federico Alberto. 2007. Cambio climatico.

Hassanzadeh, H, Pooladi-Darvish, M, Keith, DW, *et al.* 2005. Modelling of convective mixing in co storage. *Journal of Canadian Petroleum Technology*, **44**(10).

Hassanzadeh, Hassan, Pooladi-Darvish, Mehran, & Keith, David W. 2006. Stability of a fluid in a horizontal saturated porous layer: effect of non-linear concentration profile, initial, and boundary conditions. *Transport in Porous Media*, **65**(2), 193–211.

Hidalgo, Juan J, & Carrera, Jesus. 2009. Effect of dispersion on the onset of convection during CO 2 sequestration. *Journal of Fluid Mechanics*, **640**, 441–452.

Huppert, Herbert E, & Neufeld, Jerome A. 2014. The fluid mechanics of carbon dioxide sequestration. *Annual review of fluid mechanics*, **46**, 255–272.

Institute, Global CCS. *Large-scale CCS facilities*. urlhttp://www.globalccsinstitute.com/projects/large-scale-ccs-projects.

Javaheri, Mohammad, Abedi, Jalal, & Hassanzadeh, Hassan. 2010. Linear stability analysis of double-diffusive convection in porous media, with application to geological storage of CO2. *Transport in porous media*, **84**(2), 441–456.

Krevor, Samuel, Blunt, Martin J, Benson, Sally M, Pentland, Christopher H, Reynolds, Catriona, Al-Menhali, Ali, & Niu, Ben. 2015. Capillary trapping for geologic carbon dioxide storage–From pore scale physics to field scale implications. *International Journal of Greenhouse Gas Control*, **40**, 221–237.

Lindeberg, Erik, & Wessel-Berg, Dag. 2011. Upscaling studies of diffusion induced convection in homogeneous and heterogeneous aquifers. *Energy Procedia*, **4**, 3927–3934.

Nomeli, Mohammad A, Tilton, Nils, & Riaz, Amir. 2014. A new model for the density of saturated solutions of CO2–H2O–NaCl in saline aquifers. *International Journal of Greenhouse Gas Control*, **31**, 192–204.

Novotny, P, & Sohnel, O. 1988. Densities of binary aqueous solutions of 306 inorganic substances. *Journal of Chemical and Engineering Data*, **33**(1), 49–55.

Otiniando Pulido, Carlos. 2018. EE.UU. se pone a la delantera de la UE en captura de CO_2. *CincoCias*.

Pau, George SH, Bell, John B, Pruess, Karsten, Almgren, Ann S, Lijewski, Michael J, & Zhang, Keni. 2010. High-resolution simulation and characterization of density-driven flow in CO2 storage in saline aquifers. *Advances in Water Resources*, **33**(4), 443–455.

Portier, Sandrine, & Rochelle, Christopher. 2005. Modelling CO2 solubility in pure water and NaCl-type waters from 0 to 300 C and from 1 to 300 bar: Application to the Utsira Formation at Sleipner. *Chemical Geology*, **217**(3-4), 187–199.

Riaz, A, Hesse, M, Tchelepi, HA, & Orr, FM. 2006. Onset of convection in a gravitationally unstable diffusive boundary layer in porous media. *Journal of Fluid Mechanics*, **548**, 87–111.

Scuro, Sante R. 2004. *Introduction to error theory.* Tech. rept. Technical Report. College Station, TX: Texas A&M University.

Slim, Anja C. 2014. Solutal-convection regimes in a two-dimensional porous medium. *Journal of Fluid Mechanics*, **741**, 461–491.

Slim, Anja C, & Ramakrishnan, TS. 2010. Onset and cessation of time-dependent, dissolution-driven convection in porous media. *Physics of fluids*, **22**(12), 124103.

Slim, Anja C, Bandi, MM, Miller, Joel C, & Mahadevan, L. 2013. Dissolution-driven convection in a Hele–Shaw cell. *Physics of Fluids*, **25**(2), 024101.

Spycher, Nicolas, Pruess, Karsten, & Ennis-King, Jonathan. 2003. CO2-H2O mixtures in the geological sequestration of CO2. I. Assessment and calculation of mutual solubilities from 12 to 100 C and up to 600 bar. *Geochimica et cosmochimica acta*, **67**(16), 3015–3031.

Sucasas, A. L. 2018. Plastico hecho con el CO_2 del aire. *Revista retina*.

Xu, Xiaofeng, Chen, Shiyi, & Zhang, Dongxiao. 2006. Convective stability analysis of the long-term storage of carbon dioxide in deep saline aquifers. *Advances in water resources*, **29**(3), 397–407.